AFGL-TR-89-0044

AD-A218 120

# Adiabatic and Diabatic Initialization of the AFGL Global Spectral Model Using Dynamic Normal Mode and Nonlinear Normal Mode Methods

LARRY KNOWLTON
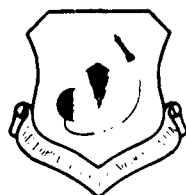DONALD NORQUIST
ROSS HOFFMAN

16 February 1989

DTIC
ELECTE
FEB 13 1990
S E D

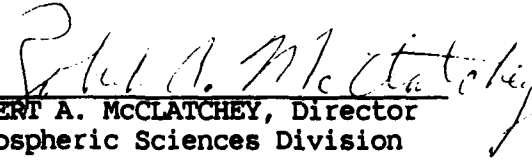ATMOSPHERIC SCIENCES DIVISION          PROJECT 2310

## AIR FORCE GEOPHYSICS LABORATORY

HANSCOM AFB, MA 01731

90 02 12 193

"This technical report has been reviewed and is approved for publication"

# REPORT DOCUMENTATION PAGE

| 1a. REPORT SECURITY CLASSIFICATION | 1b. RESTRICTIVE MARKINGS |
|---|---|
| Unclassified | |

| 2a. SECURITY CLASSIFICATION AUTHORITY | 3. DISTRIBUTION / AVAILABILITY OF REPORT |
|---|---|
| 2b. DECLASSIFICATION / DOWNGRADING SCHEDULE | Approved for public release; distribution unlimited |

| 4. PERFORMING ORGANIZATION REPORT NUMBER(S) | 5. MONITORING ORGANIZATION REPORT NUMBER(S) |
|---|---|
| AFGL-TR-89-0044 ERP No. 1022 | |

| 6a. NAME OF PERFORMING ORGANIZATION | 6b. OFFICE SYMBOL (If applicable) | 7a. NAME OF MONITORING ORGANIZATION |
|---|---|---|
| Air Force Geophysics Laboratory | LYP | |

| 6c. ADDRESS (City, State, and ZIP Code) | 7b. ADDRESS (City, State, and ZIP Code) |
|---|---|
| Hanscom Air Force Base Massachusetts 01731-5000 | |

| 8a. NAME OF FUNDING / SPONSORING ORGANIZATION | 8b. OFFICE SYMBOL (If applicable) | 9. PROCUREMENT INSTRUMENT IDENTIFICATION NUMBER |
|---|---|---|
| | | |

| 8c. ADDRESS (City, State, and ZIP Code) | 10. SOURCE OF FUNDING NUMBERS | | | |
|---|---|---|---|---|
| | PROGRAM ELEMENT NO. | PROJECT NO. | TASK NO. | WORK UNIT ACCESSION NO. |
| | 61101F | 2310 | G7 | 08 |

11. TITLE (Include Security Classification)
(U) Adiabatic and Diabatic Initialization of the AFGL Global Spectral Model Using Dynamic Normal Mode and Nonlinear Normal Mode Methods

12. PERSONAL AUTHOR(S)
Knowlton, Larry; Norquist, Donald; Hoffman, Ross*

| 13a. TYPE OF REPORT | 13b. TIME COVERED | 14. DATE OF REPORT (Year, Month, Day) | 15. PAGE COUNT |
|---|---|---|---|
| Final | FROM Oct 87 TO Sept 88 | 1989 February 16 | 46 |

16. SUPPLEMENTARY NOTATION

*AER, Inc., Cambridge, Massachusetts

| 17. | COSATI CODES | | 18. SUBJECT TERMS (Continue on reverse if necessary and identify by block number) |
|---|---|---|---|
| FIELD | GROUP | SUB-GROUP | Numerical weather prediction; Normal modes; |
| | | | Spectral atmospheric models; Global model initialization; |
| | | | Weather forecasting; Diabatic initialization. |

19. ABSTRACT (Continue on reverse if necessary and identify by block number)

Dynamic normal mode initialization (DNI) is applied to low and high resolution versions of the AFGL global spectral model. This scheme is tested against the operational nonlinear normal mode initialization (NMI) procedure using both adiabatic and diabatic forms of the model tendencies. The DNI-based forecasts are comparable in accuracy to the NMI-based forecasts, with small differences between the adiabatic and diabatic versions of each. DNI initial conditions were somewhat more damped in the divergence fields than were the NMI fields. This is believed to be due to the frequency response characteristics of the DNI's forward-backward time scheme, which tended to partially damp resolvable wavelengths.

| 20. DISTRIBUTION / AVAILABILITY OF ABSTRACT | 21. ABSTRACT SECURITY CLASSIFICATION |
|---|---|
| ☒ UNCLASSIFIED/UNLIMITED ☐ SAME AS RPT. ☐ DTIC USERS | Unclassified |

| 22a. NAME OF RESPONSIBLE INDIVIDUAL | 22b. TELEPHONE (Include Area Code) | 22c. OFFICE SYMBOL |
|---|---|---|
| Donald C. Norquist | (617) 377-2962 | AFGL/LYP |

**DD FORM 1473,** 84 MAR

83 APR edition may be used until exhausted.
All other editions are obsolete.

## Contents

## Illustrations

iv

**Tables**

v

# Adiabatic and Diabatic Initialization of the AFGL Global Spectral Model Using Dynamic Normal Mode and Nonlinear Normal Mode Methods

## 1. INTRODUCTION

Initialization, the process of balancing the analyzed mass and wind fields before a model forecast begins, to prevent contamination by high frequency gravity waves during the forecast, has attracted much attention in recent years. Various initialization schemes have evolved out of past studies, such as the static balance method, [1,2] dynamic initialization,[3] and normal mode initialization.[4] A review of various initialization schemes can be found in Daley.[5] These schemes have exhibited many individual capabilities, but also had liabilities such as the need for quasi-geostrophic assumptions and elliptic conditions (static balance method), increased computational time (dynamic initialization), convergence problems when including diabatic effects, and difficulty in application to limited area models (normal mode

1.  Charney, J. (1955) The case of the primitive equations of motion in numerical forecasting. *Tellus*, 7:22-26.
2.  Phillips, N. (1960) On the problem of initial data for the primitive equations. *Tellus*, 12:121-126.
3.  Miyakoda, K., and Moyer, R.W. (1968) A method of initialization for dynamical weather forecasting. *Tellus*, 20:115-128.
4.  Machenhauer, B. (1977) On the dynamics of gravity oscillations in a shallow water model, with application to normal mode initialization. *Beitr. Phys. Atmos.*, 50:253-271.
5.  Daley, R. (1981) Normal mode initialization. *Rev. Geophys. Space Phys.*, 19:450-468.

initialization). However, a new type of initialization demonstrated by Sugi[6] has been shown to successfully combine all the advantages and eliminate most of the disadvantages of the earlier initialization schemes. This initialization procedure is referred to as "dynamic (or implicit) normal mode initialization" (DNI). The procedure achieves damping of undesirable high frequency gravity waves by the forward-backward integration of the linear part of a model state around the initial time without the explicit computation of the model normal modes.

The performance of DNI is evaluated further in this study by applying the scheme to varius resolution versions of the AFGL global spectral model (GSM) (see Brenner et al.[7]), and comparing the forecasts obtained from DNI to those forecasts obtained from the Machenhauer nonlinear normal mode initialization (NMI) (see Ballish[8]) and a noninitialized model state (NOI). Both the VAX 8650 and CRAY 2 computer systems were employed in this study--the former for an initial low resolution "test" run of the GSM (Section 2), and the latter for the higher resolution forecasts presented in Section 3 and the full physics (diabatic) GSM runs described in Section 4.

## 2. DNI IN A LOW RESOLUTION GSM ENVIRONMENT

The first application of DNI in this study was to the low resolution (15 rhomboidal, 6 layer) baseline GSM described in Brenner et al.[7] This GSM included simple boundary-layer and convection physics as described in Sela.[9] Figure 1 is a schematic flow chart of the DNI process. The initial undamped global analysis is read by the GSM, and the nonlinear part of the full model tendencies are computed from the present model state. The routine ADDLIN adds the linear part of the full present model state tendencies to the nonlinear part from GSM to obtain new full model tendencies. Linearized present model state tendencies are computed in LINGSM, a linearized version of the adiabatic GSM,[10] which calculates linearized tendencies directly from the initial model state. After LINGSM, an update calculation of the nonlinear part of the full tendencies is performed in NLUPDATE by subtracting the linearized tendencies calculated in LINGSM from the full model tendencies

6. Sugi, M. (1986) Dynamic normal mode initialization. *J. Meteor. Soc. Japan*, **64**:623-626.
7. Brenner, S., Yang, C.H., and Yee, S.Y.K. (1982) *The AFGL Spectral Model of the Moist Global Atmosphere: Documentation of the Baseline Version.* AFGL-TR-82-0393, Air Force Geophysics Laboratory, Hanscom AFB. [NTIS ADA 129283.]
8. Ballish, A.B. (1980) *Initialization Theory and Application to the NMC Spectral Model.* Ph.D. thesis, Dept. of Meteorology, U. of Maryland.
9. Sela, J. (1980) Spectral modeling at the National Meteorological Center. *Mon. Wea. Rev..* **108**:1279-1292.
10. Sela, J. (1982) *The NMC Spectral Model.* NOAA Technical Report NWS-30.
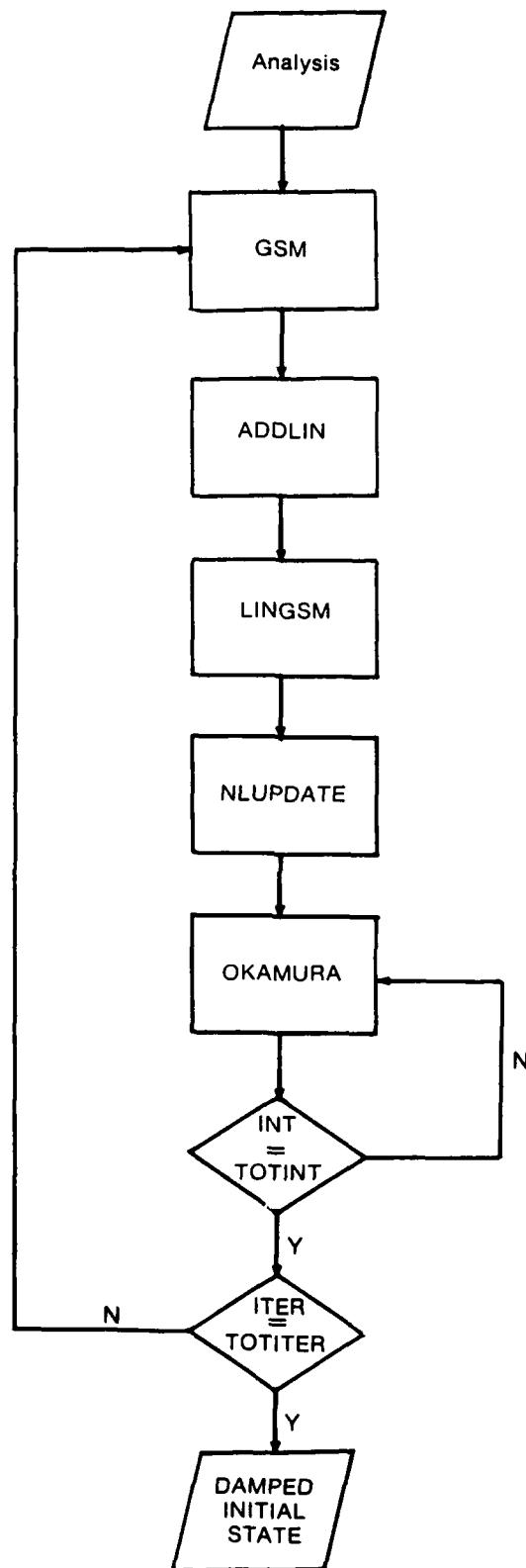
Figure 1. Schematic Diagram of DNI Process

3

calculated in ADDLIN. The linearized tendencies from LINGSM and the nonlinear part of the full tendencies are then passed into routine OKAMURA and integrated a specific number of times using the OKAMURA forward-backward selective damping scheme employed by Sugi.[6] In the forward step, the sum of the linearized tendencies and the nonlinear part of the full model tendencies are multiplied by the time step $\Delta t$ and added to the present model state. In the backward step, the sum of linearized tendencies of the forward step model state and the original nonlinear part of the full model tendencies are multiplied by $\Delta t$ and subtracted from the forward step model state. Thus, the nonlinear part of the full model tendencies is held constant during the forward-backward integration. The integrated linearized tendencies and nonlinear part of the full model tendencies form the new damped model state. Then new linearized tendencies of that damped model state are calculated in OKAMURA using LINGSM and used in the next integration. After the specified number of integrations is completed for that iteration, the damped model state is used to compute the new full model tendencies from GSM and ADDLIN, and the linearized version of these from LINGSM are subtracted to get the new nonlinear part of the full model tendencies in NLUPDATE. The process is repeated until the specified number of iterations is completed. In the Machenhauer nonlinear NMI,[8] the linear and nonlinear parts of the full tendencies are treated together in the normal mode computations during each iteration.

In this study, two iterations of the Machenhauer NMI were employed using two vertical modes. Five iterations of 11, 20, and 218 forward-backward integrations with the time steps of 598, 420, and 137 seconds, respectively, were used in three separate DNI runs. These number of integrations (n) and time steps ($\Delta t$) were computed using Sugi's Eqs. (23)-(26) where $_{max}$ was set to a value corresponding to the maximum frequency of the model normal modes. This frequency, in the case of the 6-layer, 15-rhomboidal AFGL GSM, corresponds to a period of 1.07 hours. The three values of n and t correspond to values for the response functions, $\lambda(\omega_{max})$, of -0.9, 0.0, and 0.9, respectively. The following sections present the results of low resolution initialization experiments similar to Sugi[6] for the FGGE 3A global analysis of 12 GMT 17 June 1979.

## 2.1 Numerical Experiment Results

Figures 2a and 2b show the change of the global mean square of the tendencies of surface pressure and 200 mb divergence, respectively, for the three cases of OKAMURA integrations used in this study. These quantities reveal the change of the initial state balance and the nature of the iterative convergence. In agreement with Sugi, both of these quantities show a decrease throughout the DNI process for all three cases of iterations, with the greater decrease occuring in the surface pressure tendencies; however, the decrease in the divergence is not as great as that shown by Sugi. It was not clear whether Sugi included diffusion in his initializations. If he did include diffusion, this may have contributed

a

GLB MN SQ D(LNP)/DT          INIT TIME 12Z17JUN79

$10^{-11}$

$10^{-12}$

$10^{-13}$

$10^{-14}$

$10^{-15}$

SEC-2

⊙ DT137.N218
▲ DT420.N20
+ DT598.N11

0  50  100  150  200  250  300  350  400  450  500  550  600  650  700  750  800  850  900  950 1000 1050 1100

FRWD-BKWD STEPS

b

GLB MN SQ D(DIV)/DT          INIT TIME 12Z17JUN79

$10^{-17}$

$10^{-18}$

$10^{-19}$

$10^{-20}$

$10^{-21}$

SEC-4

⊙ DT137.N218
▲ DT420.N20
+ DT598.N11

0  50  100  150  200  250  300  350  400  450  500  550  600  650  700  750  800  850  900  950 1000 1050 1100

FRWD-BKWD STEPS

Figure 2. Change of the Global Mean Square of Tendencies After DNI: (a) Surface Pressure, (b) Divergence

5

to the greater degree of damping observed in his divergence tendencies as compared to the divergence tendencies generated by the initializations in this study, which did not include diffusion.
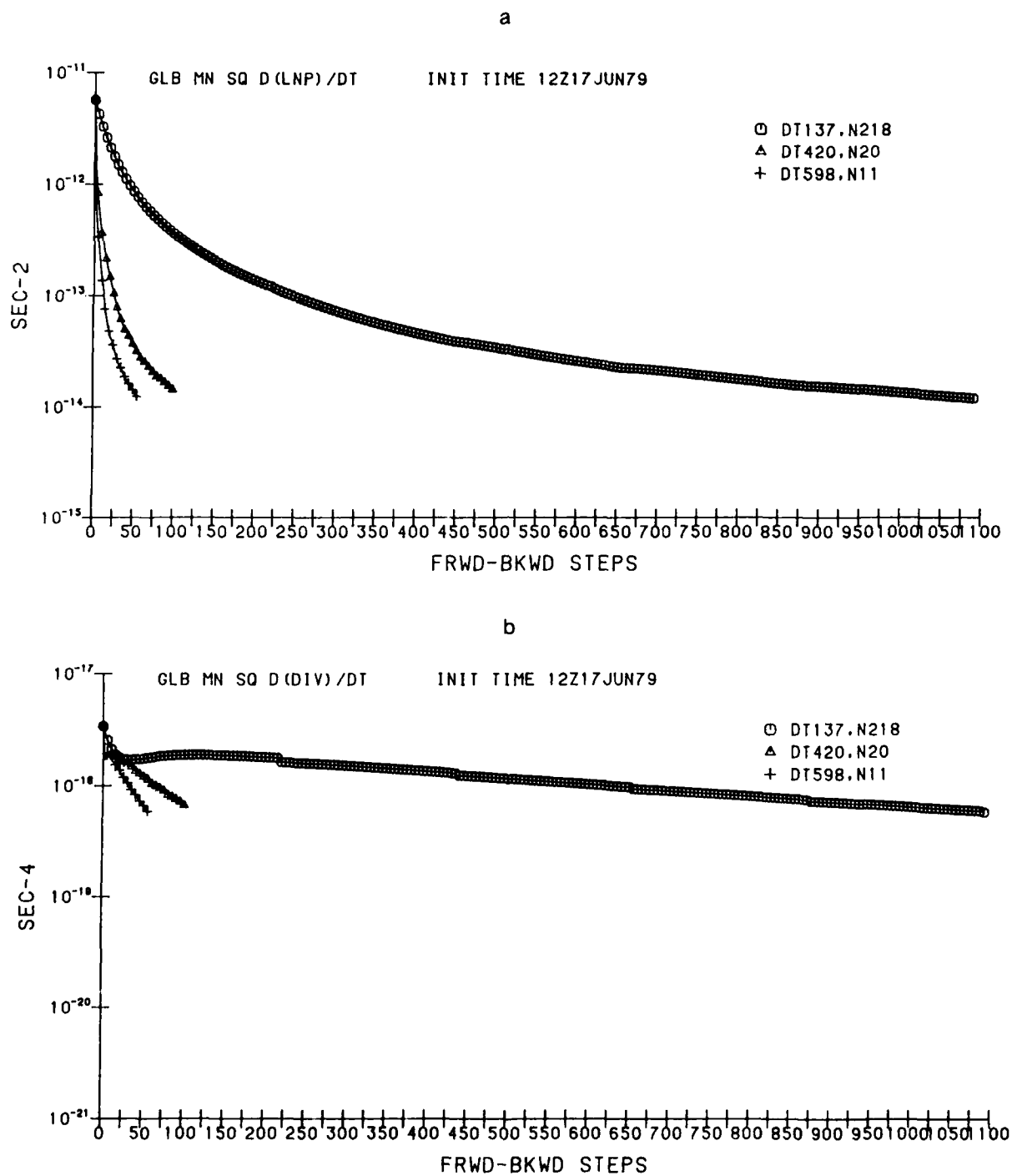
Surface pressure changes for DNI, NMI, and NOI forecasts out to 12 hours are shown in Figure 3 for six different grid points on the low resolution AFGL GSM. These six grid point locations correspond closely to the six locations in Sugi.[6] Like Sugi, the high frequency, large amplitude pressure oscillations evident in the forecasts with no model initialization are shown to be significantly damped in both the DNI and NMI initialized forecasts. The frequency of the large amplitude surface pressure oscillations for NOI in the AFGL low resolution environment are lower than those found by Sugi, most likely due to the presence of smaller scale waves being detected by the higher horizontal and vertical resolution of Sugi's GSM.

Table 1 summarizes the mass-weighted global root mean square (RMS) differences between vorticity, divergence, temperature, and surface pressure among the DNI, NMI, and NOI AFGL low resolution GSM forecasts. As in Sugi,[6] with the exception of vorticity at the initial time and 6 hours, the RMS differences between DNI and NMI are generally smaller than between DNI and NOI or NMI and NOI. It appears that, with initialization, two solutions from different initial conditions diverge less rapidly than solutions from initial states involving one with and one without initialization.

At the initial time, the RMS differences between DNI and NOI are smaller than between NMI and NOI for temperature and surface pressure but larger for vorticity and divergence. Sugi found this same trend except for divergence, and suggested that his results indicated that DNI modifies the rotational wind field more and the mass field less than NMI. Unlike Sugi's results, the divergence values in this study show the same trend as the vorticity for the DNI-NOI and NMI-NOI, suggesting that the divergent wind field is also modified more and the mass field less by DNI than by NMI.

The three plots in Figure 4 show the RMS differences between the AFGL GSM 12-hour forecasts and the corresponding FGGE 3A verifications of geopotential height, and the u and v components of the wind. It is readily apparent in Figure 4a that the DNI and NMI forecasts of geopotential height are quite similar and much better than the forecast without initialization (NOI) below 250 mb. Above 250 mb, NOI actually becomes better than NMI, but the DNI forecast remains superior to NOI up to 150 mb. RMSE values of Z in Figure 4a at levels above 150 mb are most likely the result of processes other than initialization, like pre- and post-processing of forecasts between model layers and isobaric levels. In fact, DNI presents the best forecast of the three schemes throughout the layer above 400 mb and around the 500 mb level. The NMI forecast surpasses both the DNI and NOI forecasts below 600 mb and near the 400 mb level. It appears from these results that NMI may be slightly better than DNI in geopotential height forecasts in the lower levels, while DNI provides the better upper level forecasts.

a



b
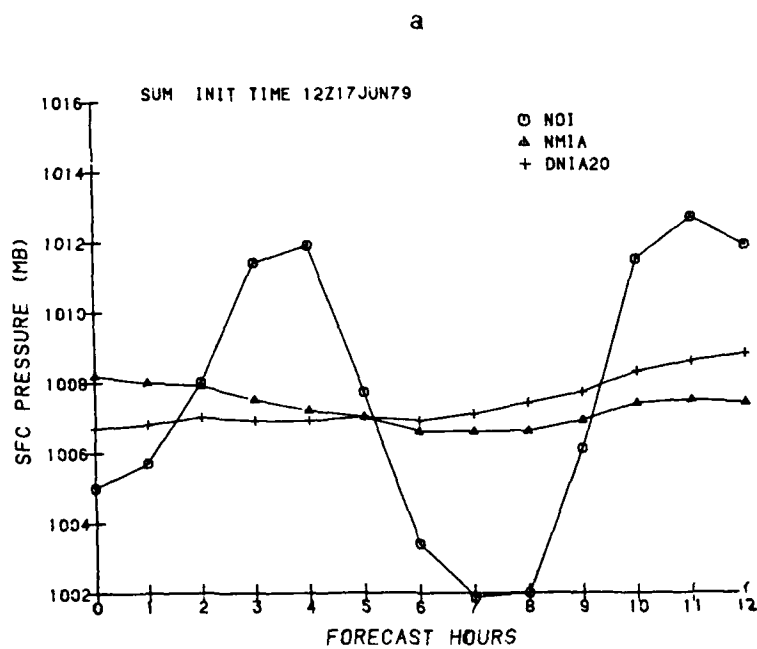


Figure 3. Surface Pressure Changes for Selected Grid Points
out to 12 Hours From 12Z 17 June 1979 for the Different Low
Resolution (15R, 6L) Initialization Methods: (a) West of Sumatra,
(b) off Chile

7

c
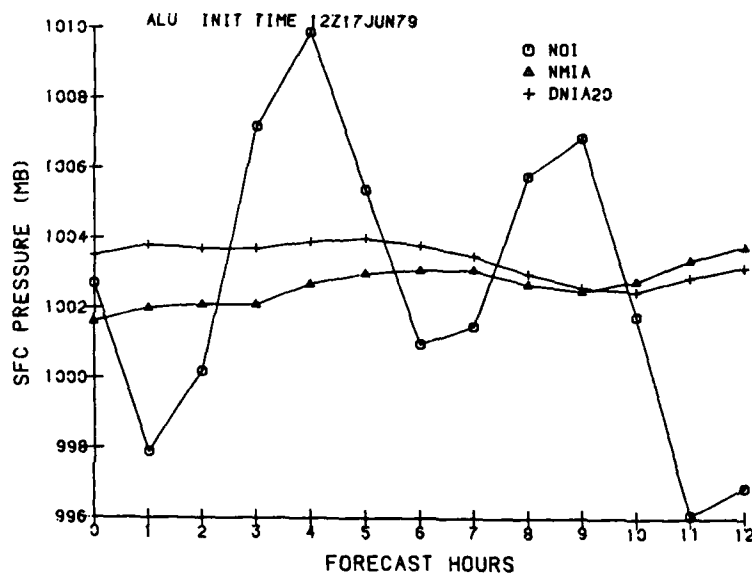


d



Figure 3 (cont). Surface Pressure Changes for Selected Grid Points
out to 12 Hours From 12Z 17 June 1979 for the Different Low
Resolution (15R, 6L) Initialization Methods: (c) South of Aleutians,
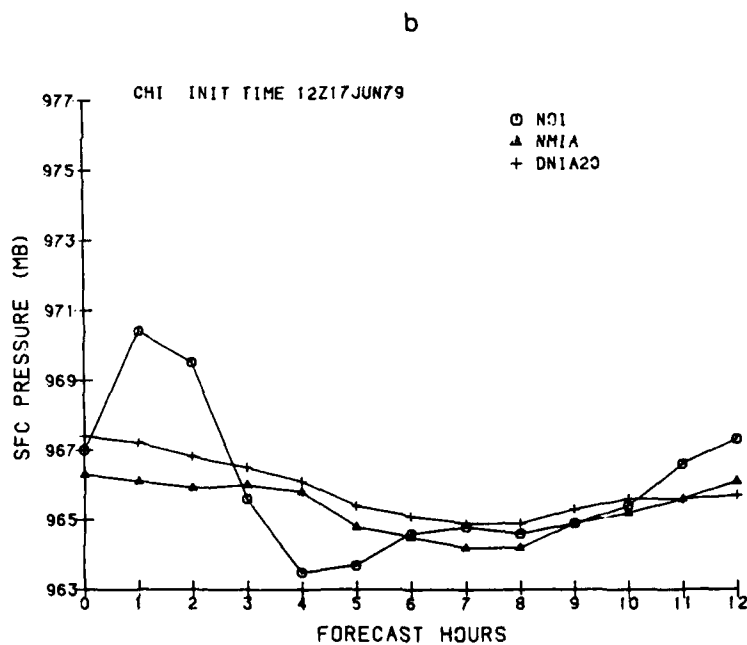(d) West of Hawaii

8
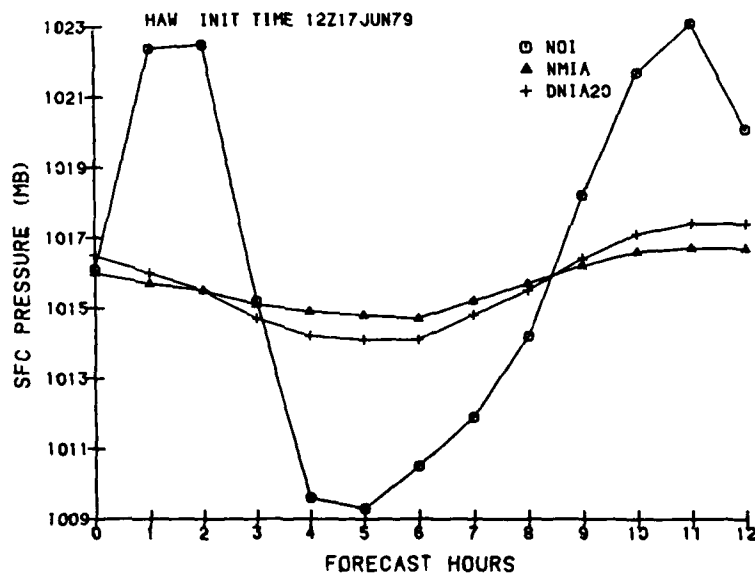
e
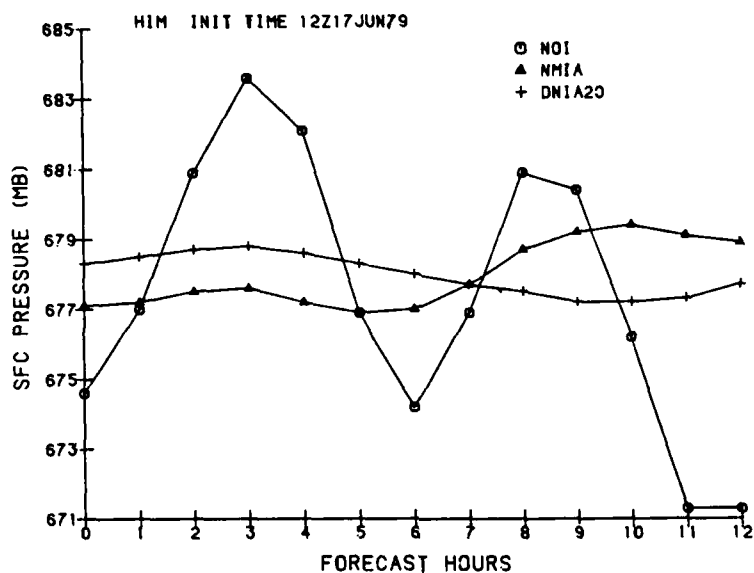


f



Figure 3 (cont). Surface Pressure Changes for Selected Grid Points out to 12 Hours From 12Z 17 June 1979 for the Different Low Resolution (15R, 6L) Initialization Methods: (e) Over the Himalayas, (f) Over Antarctica

9
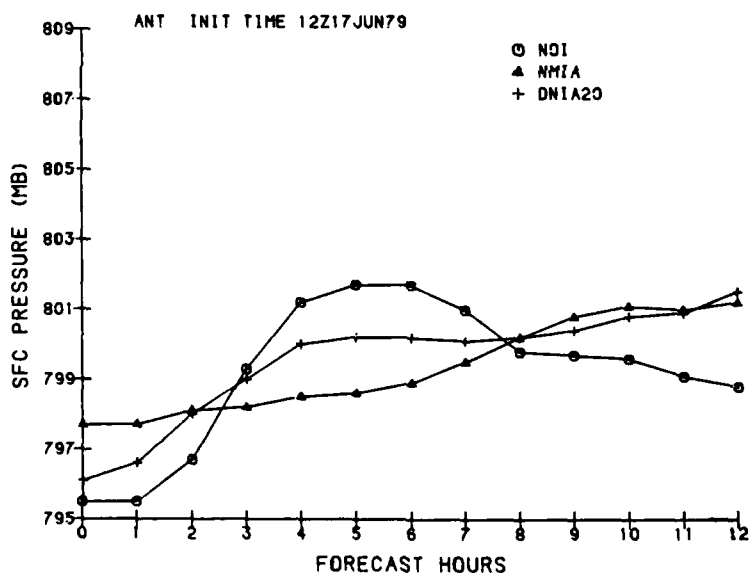
Table 1. Global RMS Differences of Vorticity $(10^{-6} \text{ sec}^{-1})$, Divergence $(10^{-6} \text{ sec}^{-1})$, Temperature (K), and Surface Pressure (mb) Among the Forecasts After Low Resolution (15R, 6L), DNI, NMI, and NOI

|       |    | DNI-NMI | DNI-NOI | NMI-NOI |
|-------|----|---------|---------|---------|
|       | 0  | 1.520   | 1.579   | 0.901   |
| VORT  | 6  | 3.631   | 3.665   | 2.614   |
|       | 12 | 2.625   | 2.870   | 2.854   |
|       | 0  | 1.475   | 3.943   | 3.466   |
| DIV   | 6  | 2.762   | 4.497   | 4.014   |
|       | 12 | 2.901   | 4.188   | 3.772   |
|       | 0  | 0.631   | 0.701   | 1.154   |
| TEMP  | 6  | 0.281   | 0.589   | 0.648   |
|       | 12 | 0.403   | 0.618   | 0.771   |
|       | 0  | 1.178   | 2.461   | 2.746   |
| SURFP | 6  | 1.104   | 3.990   | 4.377   |
|       | 12 | 1.368   | 3.113   | 3.842   |

Figures 4b and 4c reveal a consistent superiority of the DNI forecast of both the u and v components of the wind over NMI and NOI below 100 mb. As with the geopotential height forecasts, a striking feature in the u and v forecasts is the better forecast of NOI relative to NMI between 300 and 100 mb. These figures suggest that NMI may have a problem, at least in the first 12 hours, in balancing the mass and wind fields in the vicinity of the jet stream, where high wind-speeds exist.

The above DNI-based forecasts were repeated for 11 and 218 time integrations for each of the five iterations, and the results showed very little difference between those forecasts and the forecast resulting from 20 integrations of the OKAMURA scheme. This negligible difference was evident in both the surface pressure variations at grid points (as in Figure 3) and the forecast RMS differences from the verification fields. Thus, it appears that the 11-integration scheme is preferable to the 20 and certainly to the 218 integrations in terms of computational efficiency for the low resolution model. The number of iterations in
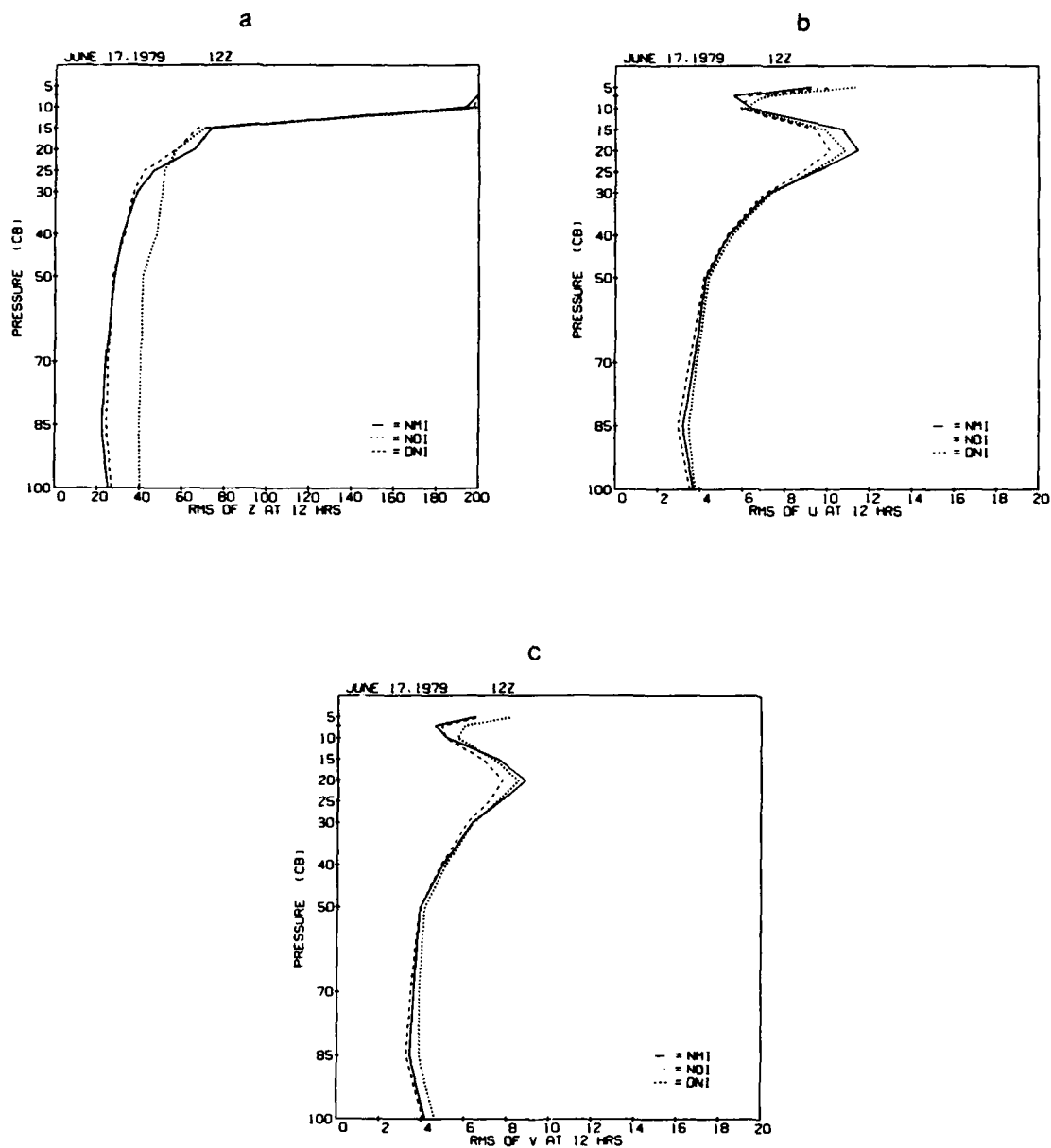
Figure 4. RMS Differences Between AFGL GSM 12 hour 15R, 6L Adiabatically Initialized Forecasts and Corresponding FGGE 3A Verifications From 12Z 17 June 1979: (a) Geopotential Height, (b) u Component of the Wind, (c) v Component of the Wind

11

the DNI were varied as well for the 11-integration case, with the results for two, three, and four iterations shown in Figure 5. The forecast u and v wind components in Figures 5a and 5b show that forecast quality improves with the number of iterations of DNI. The same is true for the height forecasts below 250 mb in Figure 5c, while above 250 mb, the lower

a

b

c

Figure 5. RMS Differences Between AFGL GSM 12 Hour 15R, 6L Adiabatically Initialized Forecasts and Corresponding FGGE 3A Verifications From 12Z 17 June 1979 for Two, Three, and Four Iterations of DNI: (a) u Component of the Wind, (b) v Component of the Wind, (c) Geopotential Height

12

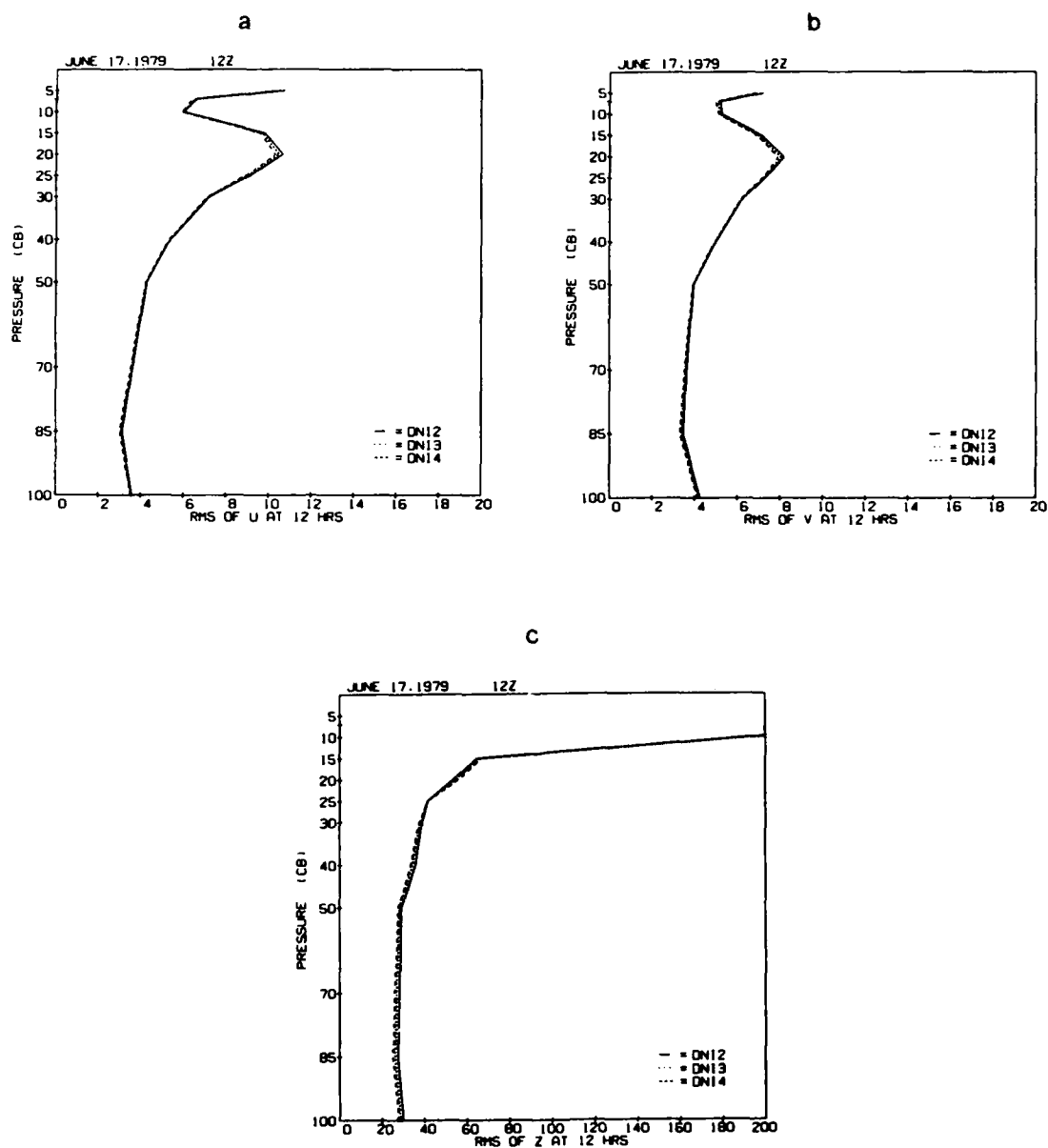iteration DNI provides a slightly better forecast. This trend in the DNI-based wind and height forecasts continues to five iterations as shown when comparing Figure 5 with Figure 4.

Boundary layer fluxes of sensible heat from oceans and momentum from oceans and land, as specified in Brenner et al.,[7] were included in the initializations for comparison to the adiabatic initializations. The resulting forecasts from these fields gave results very similar to the forecasts originating from initializations without the addition of these boundary layer processes. This suggests that simple parameterization of sensible heat fluxes from oceans and momentum fluxes from both oceans and land has negligible impact on the initialized state in the low resolution GSM.

## 3. DNI IN A HIGH RESOLUTION GSM ENVIRONMENT

### 3.1 Adiabatic Initialization

Two high resolution (12 layer, 40 rhomboidal, and 15 layer, 40 rhomboidal) GSM adiabatic initialization experiments used DNI and NMI numerical experiments similar to those described in Section 2.1. The 12-layer, 40-rhomboidal GSM physics featured only simple boundary-layer and convection physics similar to the low resolution GSM in Section 2, while the 15-layer, 40-rhomboidal GSM included radiation physics[11] in addition to more complex convection[12] and boundary layer[13] physics. Whereas forecasts generated from initialized fields included these physical effects, none of these physical effects were included in the adiabatic initialization process. The sigma thicknesses of the model layers for the 12-layer case were identical to those of Brenner et al.[14] Those of the 15-layer case were identical from the top of the atmosphere down to sigma = 0.8, where the two coarse layers were replaced by five thinner layers necessary to support the more sophisticated boundary-layer physics.

Using the same equations from Sugi[6] as in the low resolution model, the corresponding n and $\Delta t$ values for the high resolution DNI initializations were determined to be 80 and 225, respectively, for a response function $\lambda(\omega_{max})$ value of -0.9. The higher

11. Ou, S.-C., and Liou, K.-N. (1988) *Development of Radiation and Cloud Parameterization Programs for AFGL Global Models.* Final Report, AFGL-TR-87-0246, Air Force Geophysics Laboratory, Hanscom AFB. AD A199440.

12. Soong, S.-T, Ogura, Y., and Kau, W.-S. (1985) *A Study of Cumulus Parameterization in a Global Circulation Model.* Final Report, AFGL-TR-85-0160, Air Force Geophysics Laboratory, Hanscom AFB. AD A170137.

13. Mahrt, L., Pan, H.-L., Ruscher, P., and Chu, C.-T. (1987) *Boundary Layer Parameterization for a Global Spectral Model.* Final Report, AFGL-TR-87-0246, Air Force Geophysics Laboratory, Hanscom AFB. AD A199440.

14. Brenner, S., Yeng, C.H., and Mitchell, K. (1984) *The AFGL Global Spectral Model: Expanded Resolution Baseline Version.* AFGL-TR-84-0308, Air Force Geophysics Laboratory, Hanscom AFB. [NTIS ADA 160370.]

number of integrations and smaller time step required for the high resolution DNI for the same response function value is expected due to the increased number of modes to be initialized. Five iterations of the DNI were used for the high resolution adiabatic experiments, and the NMI used two iterations in normalizing four vertical modes. In addition to the June case used for the low resolution initialization, high resolution GSM initialization forecast verification experiments were performed on the FGGE 3A global analyses of 12 GMT 17 February 1979.

Table 2 presents the high resolution (12 layer, 40 rhomboidal) equivalent of Table 1 in Section 2.1 for 0, 12, and 24 hours. As with the low resolution initializations in this study, and in agreement with the results in Sugi,[6] the RMS differences between DNI and NMI are generally smaller than those between DNI and NOI or NMI and NOI. The RMS differences between DNI and NOI are smaller than those between NMI and NOI at the initial time except for vorticity, paralleling Sugi's results and supporting his hypothesis that DNI modifies the rotational wind field more and the mass field less than NMI. With the exception of the DNI-NMI temperature, the RMS differences in Table 2 all increase between 0 and 12 hours. This result is consistent with both Sugi's and this study's low resolution RMS differences, except for DNI-NOI divergence in the former and the DNI-NOI and NMI-NOI temperatures in the latter. By 24 hours, the RMS differences have decreased their rate of increase or, as in DNI-NOI temperature and pressure and NMI-NOI pressure, have actually decreased in magnitude from their 12-hour values, indicating a gradual decrease in the impact of the DNI and NMI on the forecast as the forecast period increases. This trend is also apparent in Sugi's results and this study's low resolution initializations described in Section 2.

It is evident from Table 2 that, except for DNI-NOI surface pressure, the magnitudes of the RMS differences are significantly greater than those observed for the low resolution GSM in Table 1. This departure may be due to the difference in resolution between the two models. Greater variations in the initializations and subsequent forecasts can be expected to occur in the higher resolution model because smaller scale waves with stronger mass and wind gradients appear; however, the values in Table 2 also exceed those found by Sugi, whose GSM resolution was similar to the high resolution GSM used in this study. The possible use of diffusion by Sugi in his initializations may account for his lower RMS difference magnitudes.

The high resolution (12 layer, 40 rhomboidal) surface pressure forecast traces out to 96 hours in Figure 6 are for the same six locations used in Sugi[6] and the low resolution surface pressure traces in Figure 3 of Section 2.1. In agreement with Sugi and the low resolution results, the high resolution pressure forecast traces reveal the strong damping effects of both DNI and NMI on the high frequency, large amplitude pressure variations of the NOI forecasts. The periods of the NOI, NMI, and DNI pressure oscillations out to 12 hours in Figure 6 are similar to those of Sugi's 12-hour pressure forecasts, though the amplitudes of the former are generally greater than the latter. The decreasing impact of DNI

14

and NMI on the longer range surface pressure forecasts becomes evident in Figure 6 as the period and amplitude of the NOI pressure oscillations decreases significantly after 24 hours and the variation between the NOI forecasts and the forecasts with DNI and NMI decrease.

Table 2. Global RMS Differences of Vorticity $(10^{-6}\ sec^{-1})$, Divergence $(10^{-6}\ sec^{-1})$, Temperature (K), and Surface Pressure (mb) Among the Forecasts After High Resolution (40R, 12L), DNI, NMI, and NOI

|       |    | DNI-NMI | DNI-NOI | NMI-NOI |
|-------|----|---------|---------|---------|
|       | 0  | 1.665   | 1.904   | 1.664   |
| VORT  | 12 | 4.291   | 5.573   | 6.735   |
|       | 24 | 6.236   | 7.400   | 9.386   |
|       | 0  | 3.727   | 4.982   | 5.511   |
| DIV   | 12 | 5.042   | 8.268   | 9.454   |
|       | 24 | 6.736   | 9.382   | 12.319  |
|       | 0  | 0.591   | 1.057   | 1.287   |
| TEMP  | 12 | 0.570   | 1.237   | 1.402   |
|       | 24 | 0.643   | 1.184   | 1.412   |
|       | 0  | 0.914   | 2.566   | 2.826   |
| SURFP | 12 | 1.326   | 4.399   | 4.691   |
|       | 24 | 1.412   | 3.858   | 4.331   |

Figures 7-10 show the RMS differences between the AFGL high resolution (40R, 12L, and 40R, 15L) GSM 12- and 24-hour forecasts from 12Z 17 February 1979 and 12Z 17 June 1979 and the corresponding FGGE 3A verification of geopotential height, and the u and v components of the wind. Like the AFGL low resolution (15R, 6L) GSM forecasts from 12Z 17 June 1979 in Section 2, the high resolution DNI and NMI 12-hour forecsts from both 12Z 17 June 1979 and 17 February 1979 are quite similar and significantly better than the forecasts without initialization (NOI). In fact, the superiority of the NOI 300-100 mb forecasts over those of the NMI exhibited in the low resolution forecasts disappears in the high resolution forecasts. The superior upper level DNI and lower level NMI geopotential

15
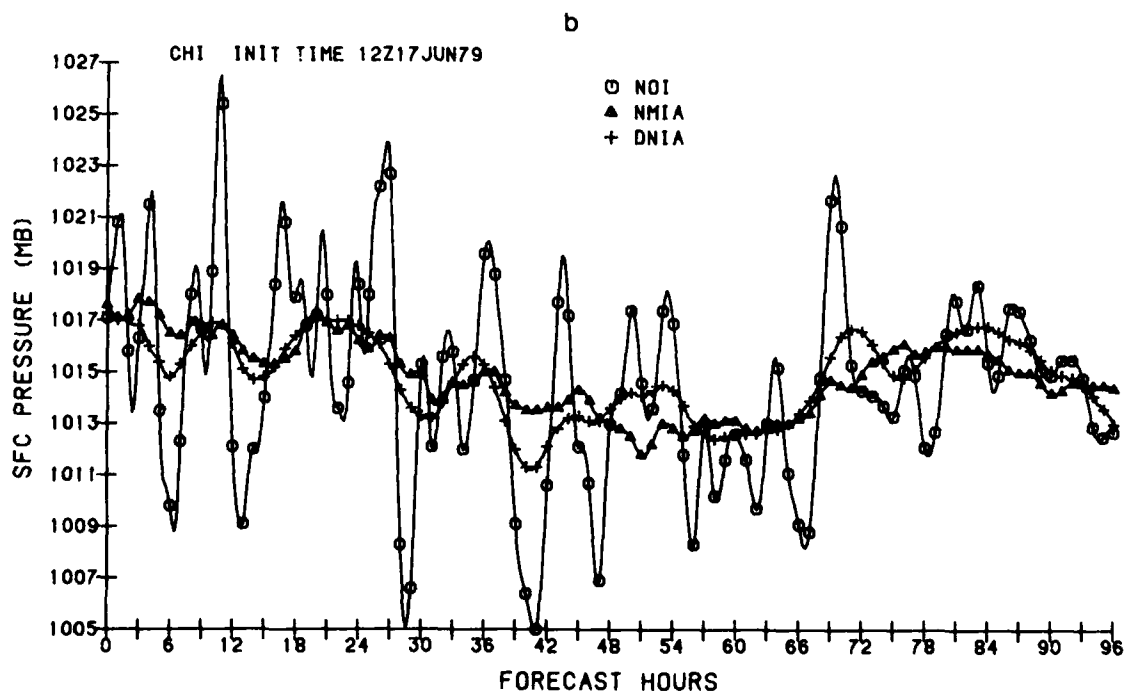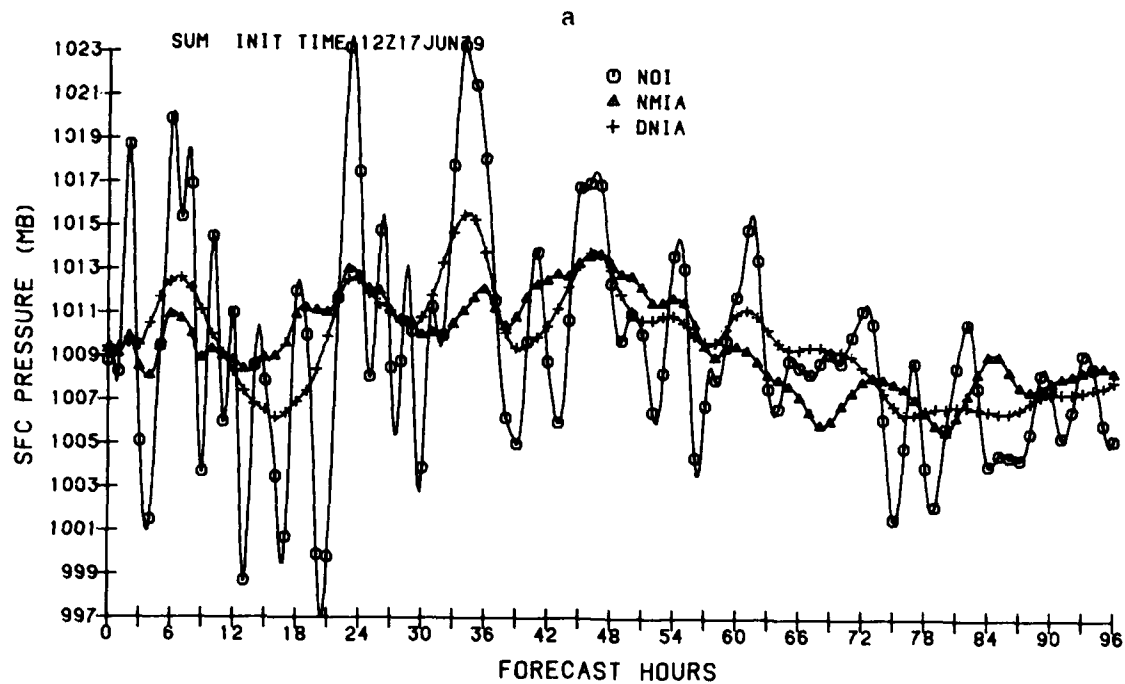
Figure 6. Surface Pressure Changes for Selected Grid Points out to 96 Hours From 12Z 17 June 1979 for the Different High Resolution (40R, 12L) Initialization Methods: (a) West of Sumatra, (b) off Chile

16
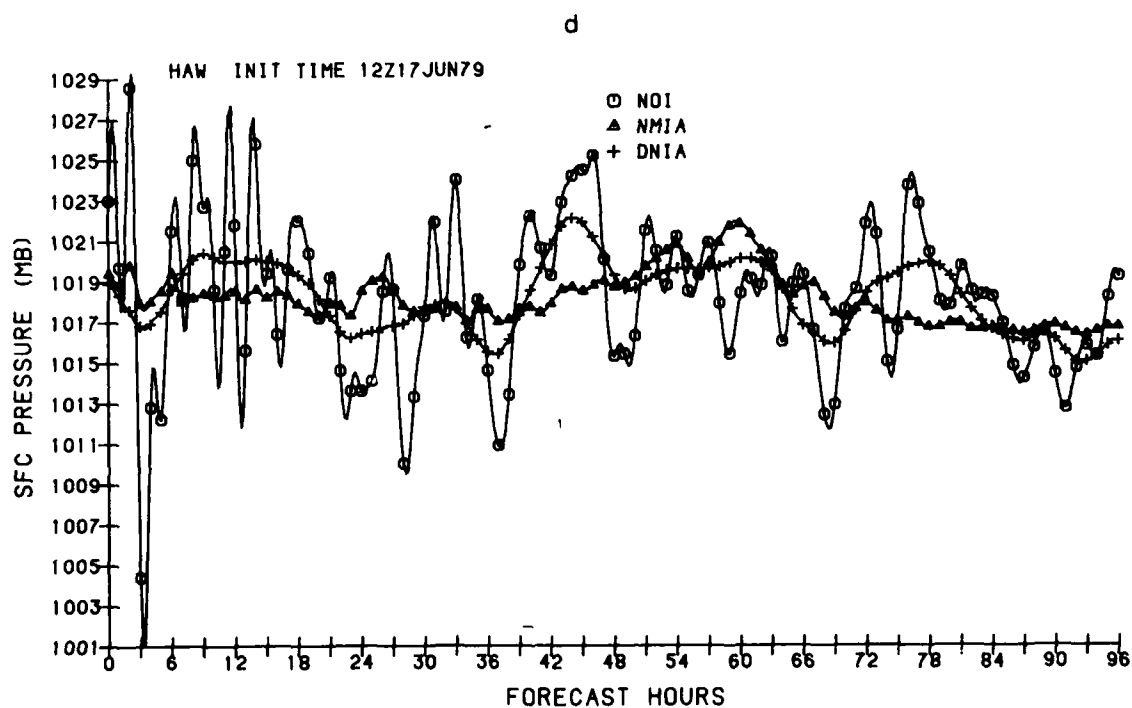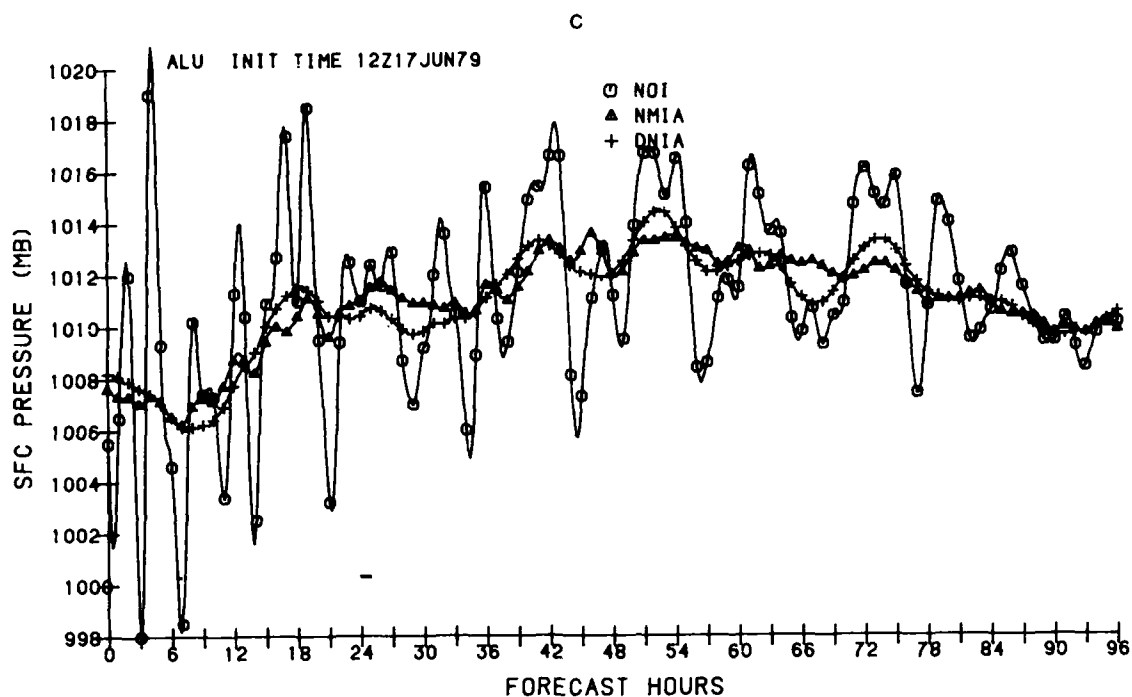
Figure 6 (cont). Surface Pressure Changes for Selected Grid Points out to 96 Hours From 12Z 17 June 1979 for the Different High Resolution (40R, 12L) Initialization Methods: (c) South of Aleutians, (d) West of Hawaii

Figure 6 (cont). Surface Pressure Changes for Selected Grid Points out to 96 Hours From 12Z 17 June 1979 for the Different High Resolution (40R, 12L) Initialization Methods: (e) Over the Himalayas, (f) Over Antarctica
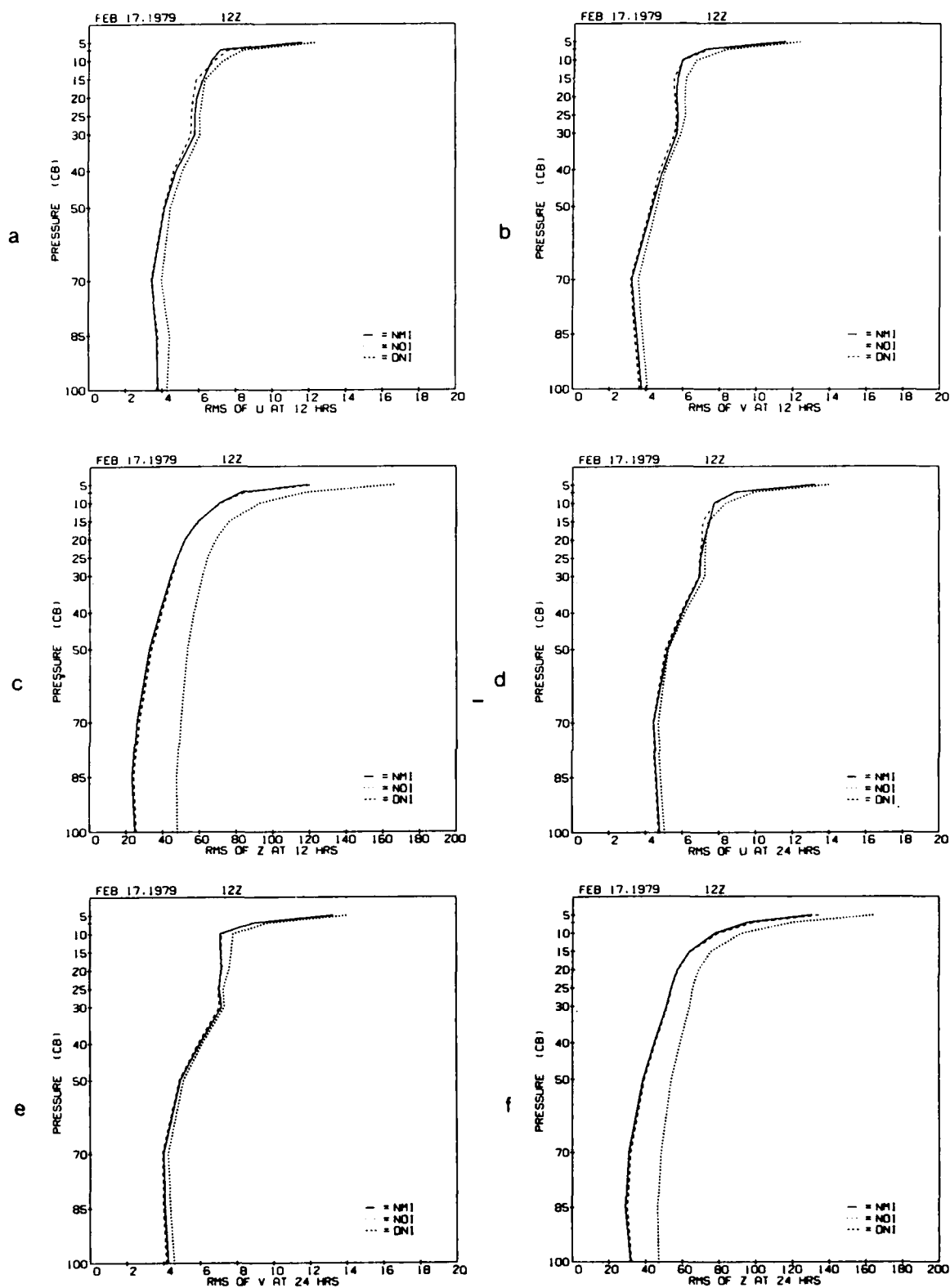
Figure 7. RMS Differences Between AFGL 40R, 12L (GWC) GSM 12- and 24-Hour Adiabatically Initialized Forecasts and Corresponding FGGE 3A Verifications From 12Z 17 February 1979: (a, d) u Component of the Wind, (b, e) v Component of the Wind, (c, f) Geopotential Height, Using Different Methods of Initialization

19

Figure 8. RMS Differences Between AFGL 40R, 12L (GWC) GSM 12- and 24-Hour
Adiabatically Initialized Forecasts and Corresponding FGGE 3A Verifications From 12Z 17
June 1979: (a, d) u Component of the Wind, (b, e) v Component of the Wind, (c, f)
Geopotential Height Using Different Methods of Initialization

20

Figure 9. RMS Differences Between AFGL 40R, 15L (ALL) GSM 12- and 24-Hour
Adiabatically Initialized Forecasts and Corresponding FGGE 3A Verifications From 12Z 17
February 1979: (a, d) u Component of the Wind, (b, e) v Component of the Wind, (c, f)
Geopotential Height Using Different Methods of Initialization

21

Figure 10. RMS Differences Between AFGL 40R, 15L (ALL) GSM 12- and 24-Hour Adiabatically Initialized Forecasts and Corresponding FGGE 3A Verifications From 12Z 17 June 1979: (a, d) u Component of the Wind, (b, e) v Component of the Wind, (c, f) Geopotential Height Using Different Methods of Initialization

22

height forecasts observed in the low resolution 12-hour forecast is also apparent in the June high resolution 12-hour geopotential height forecasts. But this discrepancy between DNI and NMI disappears in the 24-hour June high resolution forecast and is nonexistent in the 12- and 24-hour February high resolution forecasts. Thus, it appears any preference of DNI or NMI to a particular level of the atmosphere is case dependent and disappears after 24 hours of forecast time. In fact, high resolution forecasts were run out to 96 hours for both the February and June cases, and the discrepancy of the RMS difference between forecast and analysis of geopotential height and u and v component of the winds among the DNI, NMI, and NOI forecasts became smaller with increased forecast time. This decreased impact of initialization with increased forecast range was also found by Brenner et al.[14] for velocity potential forecasts using NMI and NOI. They concluded that the damping effects of the semi-implicit time scheme and subgrid scale diffusion in the AFGL GSM adequately controls high frequency gravity waves beyond 24 hours. Thus, the primary application for initialization of forecast models is in their use as "first-guess" models in intermittent data assimilation processes where the accuracy of very short-term (6-12 hour) forecasts is important.

### 3.2 Diabatic Initialization

Diabatic initializations were performed incorporating initial model tendencies contributed by each of the simple and complex physics packages used in the 12- and 15-layer GSM forecasts, respectively, in addition to the adiabatic part of the tendencies as used above. For the diabatic initialization study, five iterations of both the DNI and NMI were performed, as opposed to the five iterations of DNI and two iterations of NMI used in the adiabatic study. Five iterations of the diabatic NMI were performed to assure convergence of the scheme, since divergence of the scheme has been observed in other diabatic NMI studies. As was done in the adiabatic NMI, four vertical modes were initialized in the diabatic NMI.

The February and June case study RMS differences between forecasts and verifications are shown in Figures 11-14 for both the 12- and 15-layer GSM model runs with diabatic NMI and DNI (hereafter called NMID and DNID). The NOI, DNI, and NMI RMS difference plots presented in Section 3.3 are repeated in Figures 11-14 for comparison with the diabatic initializations. There is very little difference between the forecasts derived from NMI and DNI and those from the NMID and DNID, though it is obvious that the initialized forecasts are superior to the noninitialized forecasts. Thus, according to the results in this study, the inclusion of physics in initialization does not appear to benefit or worsen the forecast, at least in a globally averaged sense.

Figures 15 and 16 show the 0-, 12-, and 24-hour global RMS divergence values from the June and February cases for both the 12-layer GWC simple physics and 15-layer complex (ALL) physics adiabatic and diabatic initialization runs. As expected from the damping characteristics of initialization, the initialized forecasts exhibit lower RMS values

Figure 11. RMS Differences Between AFGL 40R, 12L (GWC) GSM 12- and 24-Hour Diabatically Initialized Forecasts and Corresponding FGGE 3A Verifications From 12Z 17 February 1979: (a, d) u Component of the Wind, (b, e) v Component of the Wind, (c, f) Geopotential Height Using Different Methods of Initialization
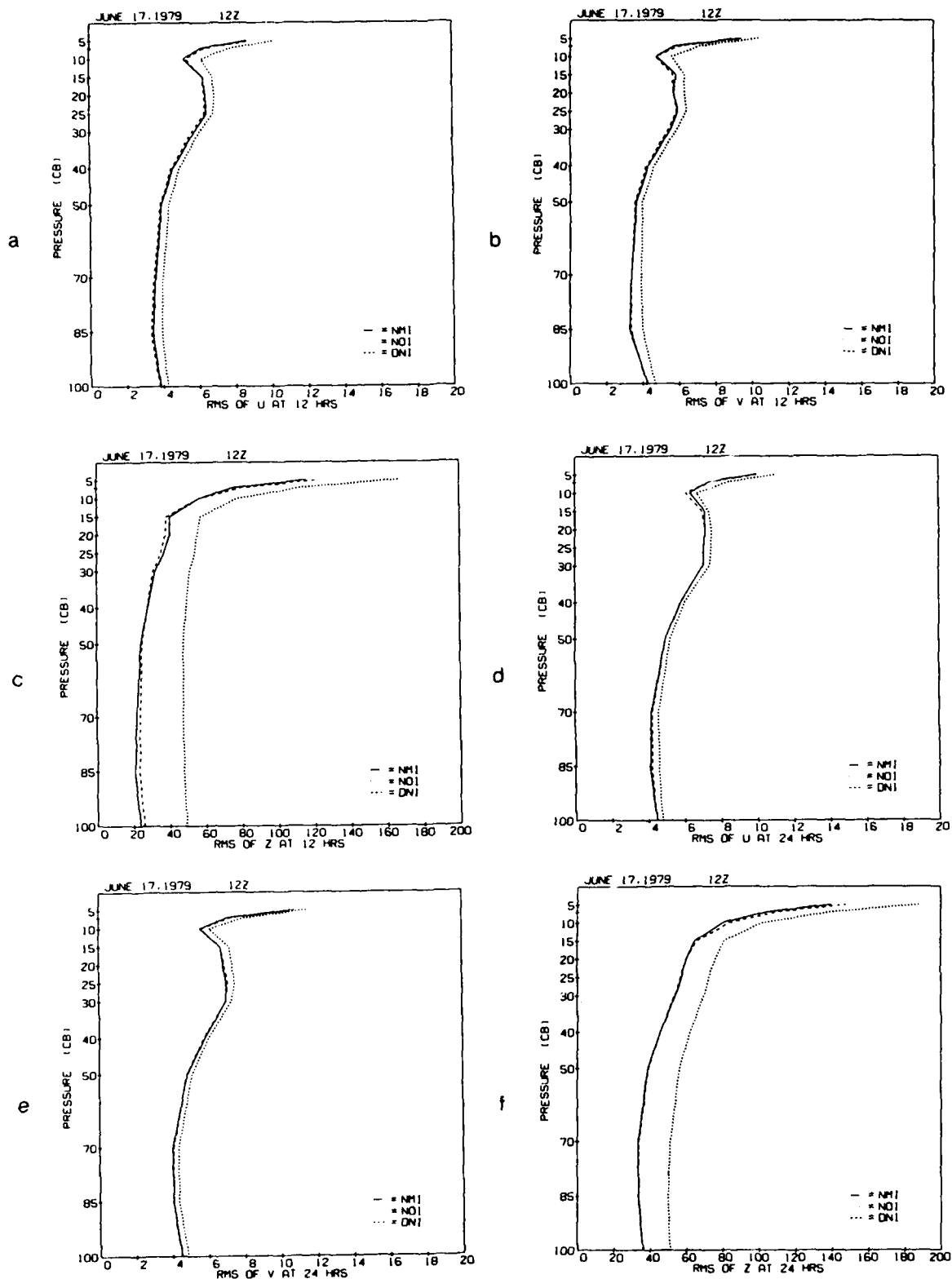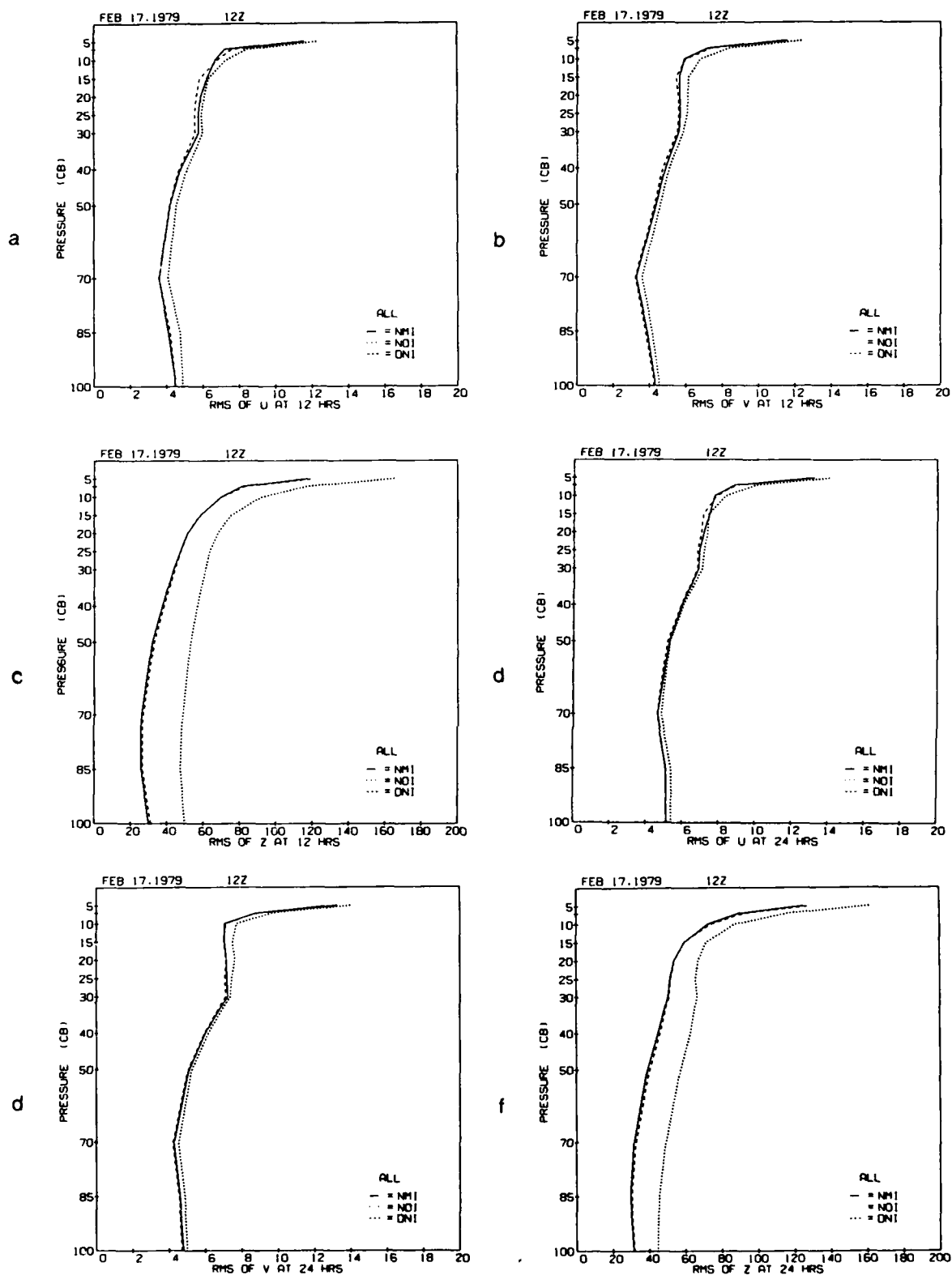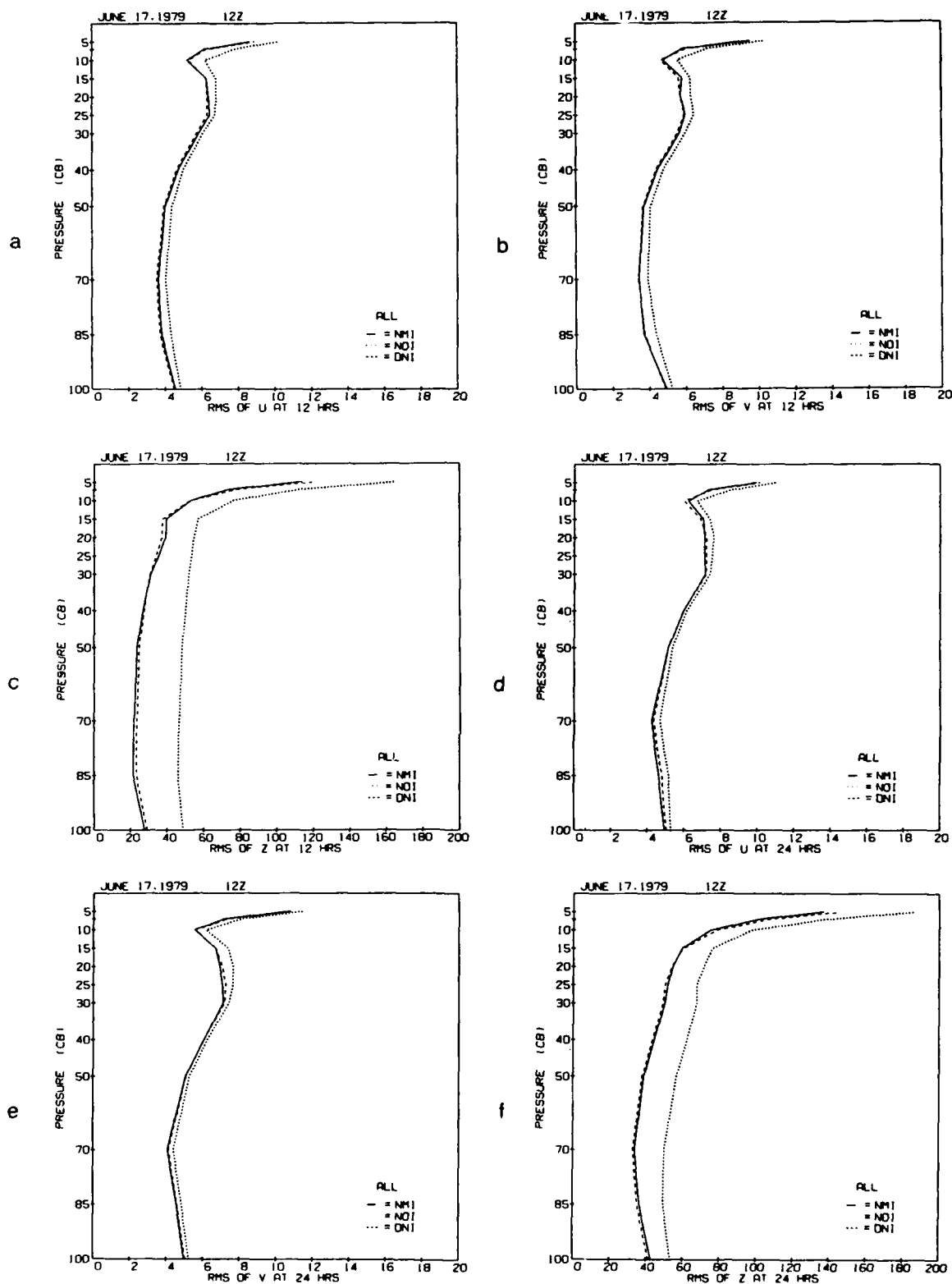
24
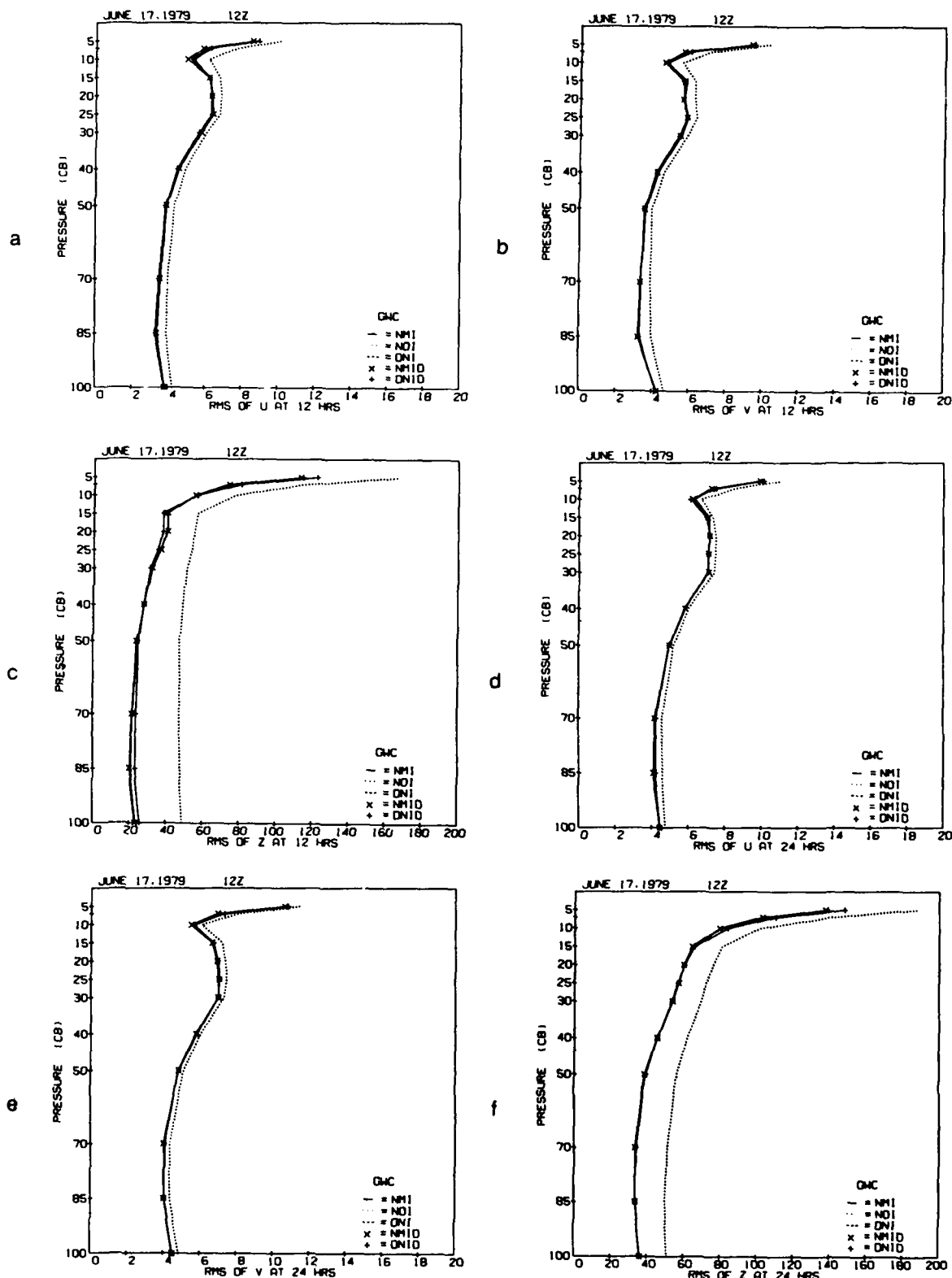
Figure 12. RMS Differences Between AFGL 40R, 12L (GWC) GSM 12- and 24-Hour
Diabatically Initialized Forecasts and Corresponding FGGE 3A Verifications From 12Z 17
June 1979: (a, d) u Component of the Wind, (b, e) v Component of the Wind, (c, f)
Geopotential Height Using Different Methods of Initialization

25
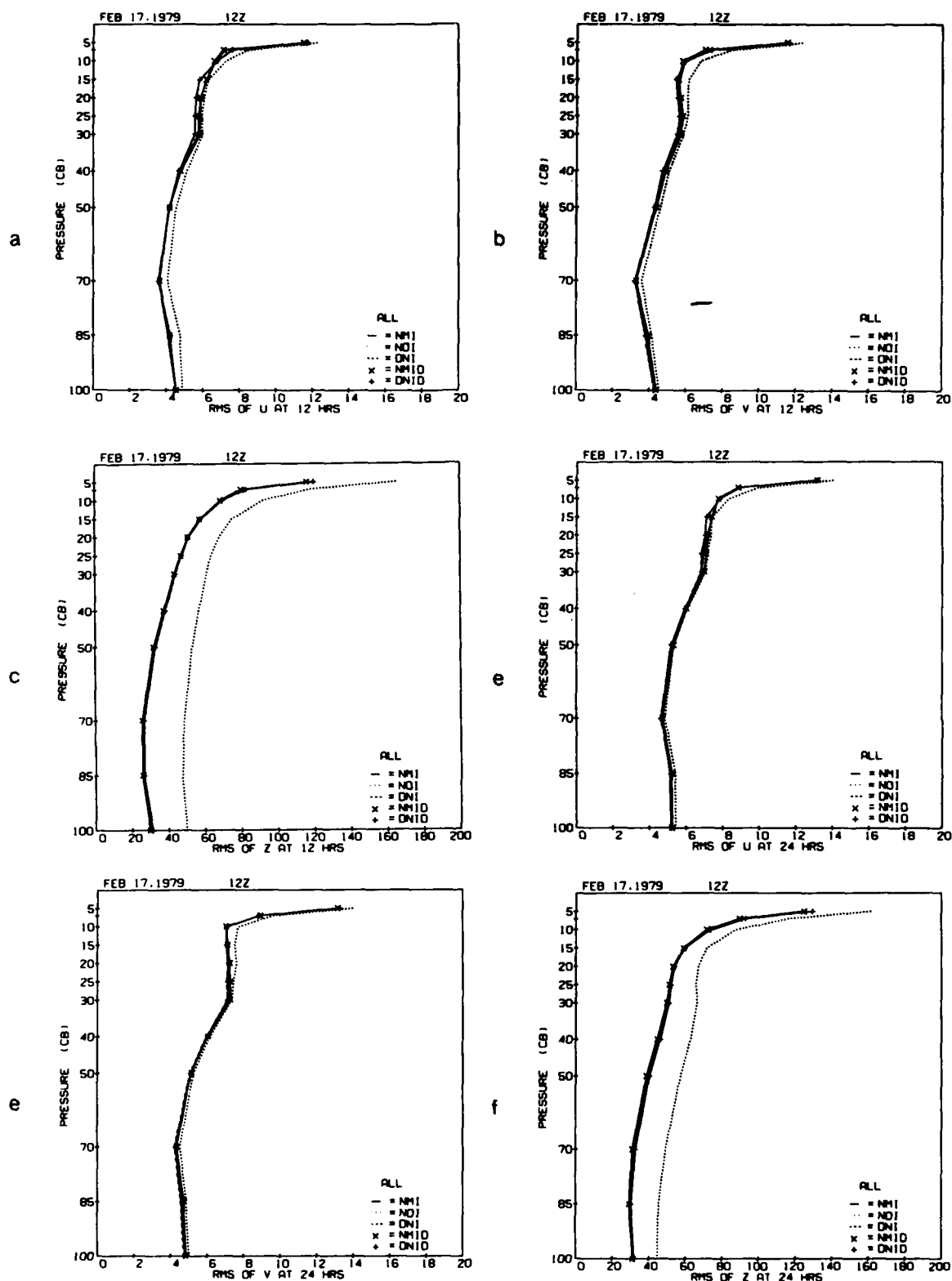
Figure 13. RMS Differences Between AFGL 40R, 15L (ALL) GSM 12- and 24-Hour Diabatically Initialized Forecasts and Corresponding FGGE 3A Verifications From 12Z 17 February 1979: (a, d) u Component of the Wind, (b, e) v Component of the Wind, (c, f) Geopotential Height Using Different Methods of Initialization
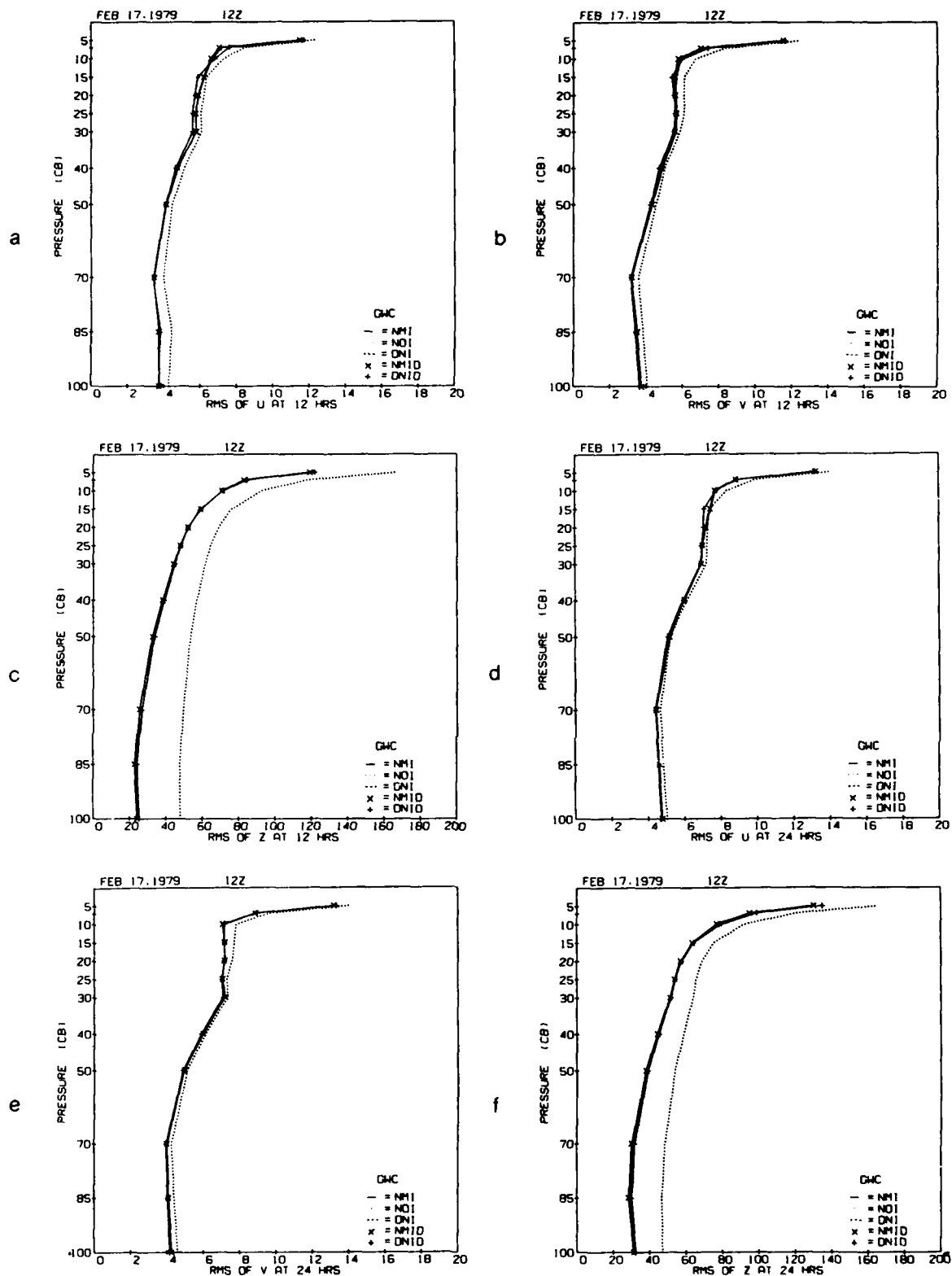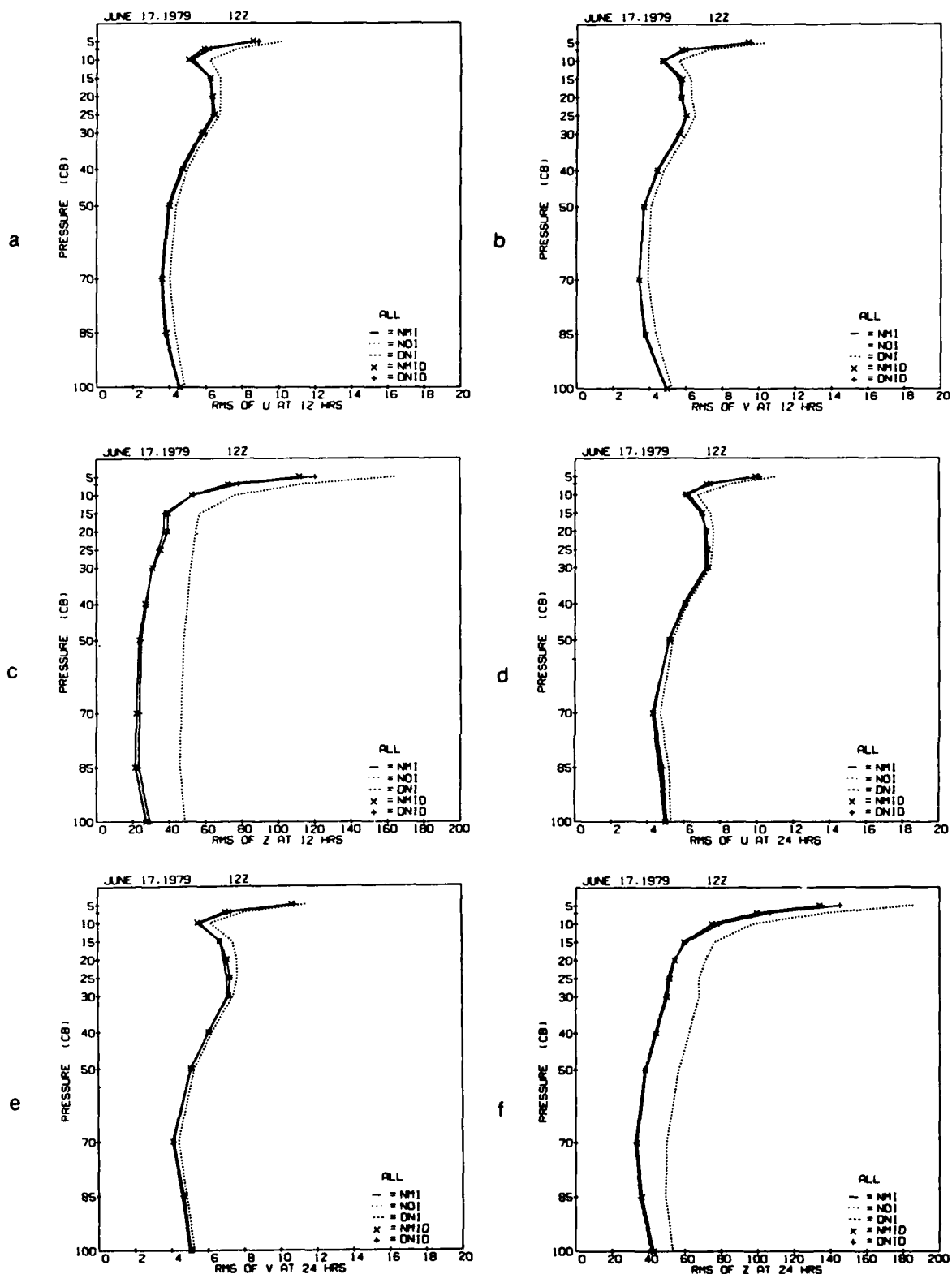
Figure 14. RMS Differences Between AFGL 40R, 15L (ALL) GSM 12- and 24-Hour
Diabatically Initialized Forecasts and Corresponding FGGE 3A Verifications From 12Z 17
June 1979: (a, d) u Component of the Wind, (b, e) v Component of the Wind, (c, f)
Geopotential Height Using Different Methods of Initialization

27
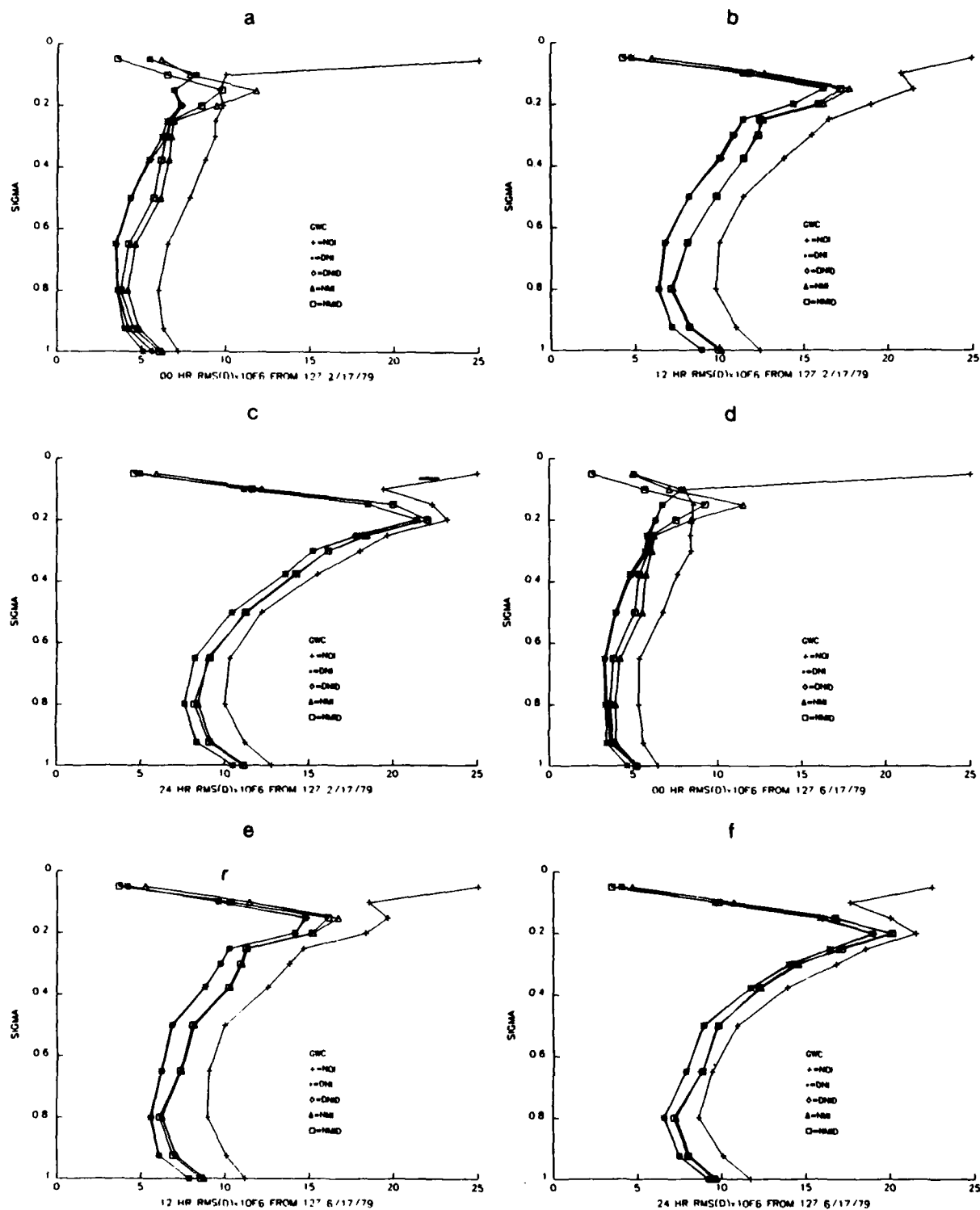
Figure 15. Vertical Profiles of 40R, 12L (GWCD) Forecast RMS Divergence Beginning
From 12Z 17 February 1979 and 12Z 17 June 1979 Using Different Methods of Initialization:
(a, d) 0 Hour, (b, e) 12 Hour, (c, f) 24 Hour
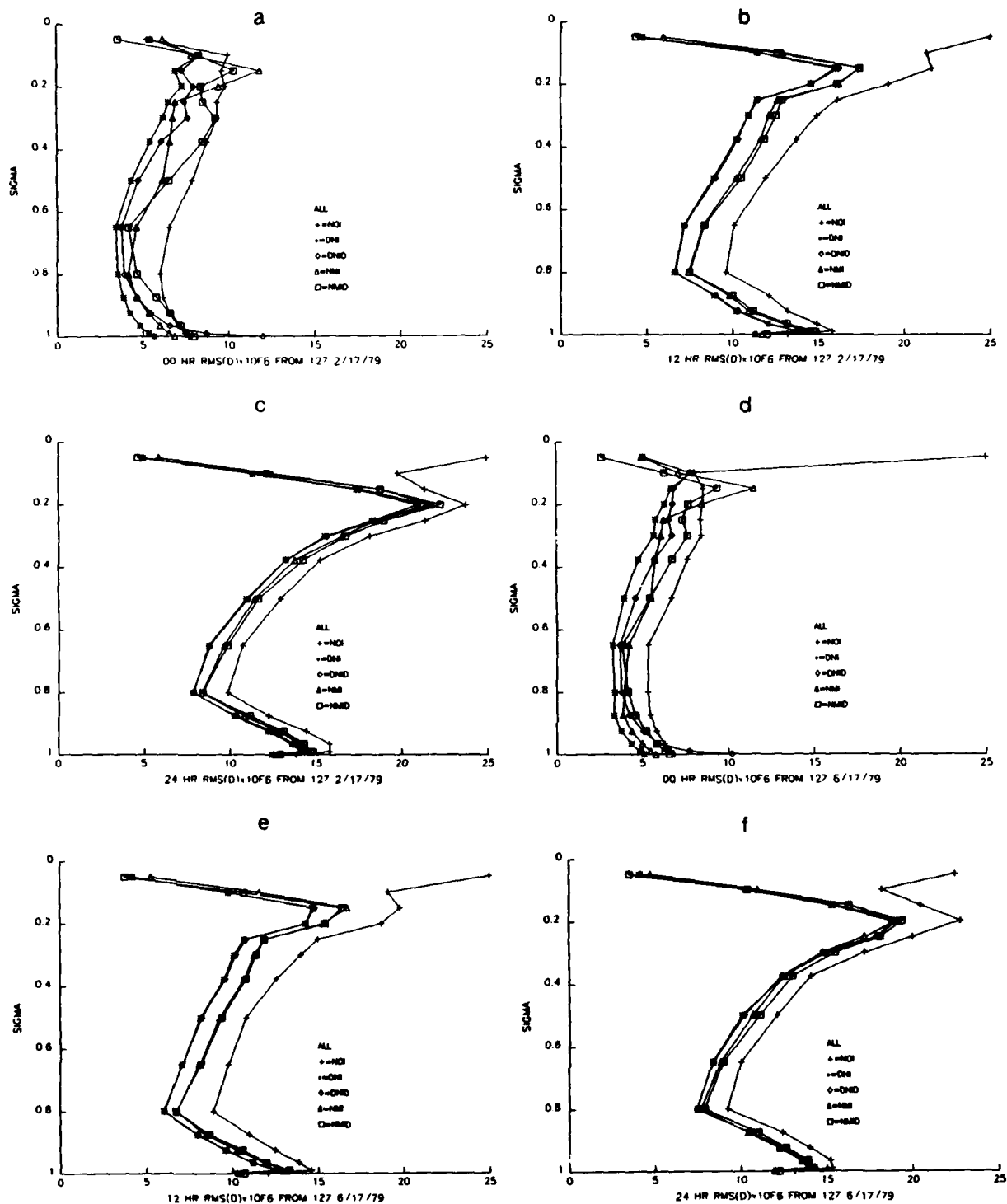
Figure 16. Vertical Profiles of 40R, 15L (ALL) Forecast RMS Divergence Beginning From 12Z 17 February 1979 and 12Z 17 June 1979 Using Different Methods of Initialization: (a, d) 0 Hour, (b, e) 12 Hour, (c, f) 24 Hour

than the noninitialized forecasts at the initial time, with the exception of the lowest two model layers in the DNID 15-layer forecast and the third highest layer in the NMI and NMID 12- and 15-layer forecasts. The more sophisticated low level physics in the 15-layer diabatic initialization may be responsible for the greater low level RMS divergence values in the DNID. The reason for the upper level RMS divergence anomalies in the NMI and NMID are not as apparent. These anomalies disappear by 12 hours due to the damping inherent in the forecast model itself. The very large value of RMS divergence observed at the top level in the NOI at the initial time is due to extrapolation error in the preprocessing of the analysis data. This erroneous divergence is damped successfully by the initialization schemes and to a lesser extent by the forecast model damping.

The 15-layer DNID RMS divergence values are closer than those of the DNI to the NOI values at the initial time. Thus, DNID in this case damps the original analysis less than the DNI does, leaving an initial state that perhaps retains divergence potentially important to the model forecast. The same is true for 15-layer NMID when compared to NMI. In fact, NMID damps the analysis less than any of the other initialization schemes for the 15-layer case. In the 12-layer case, NMI damps less than NMID, but the 12-layer physics are less sophisticated than the 15-layer physics and may account for this discrepancy.

A possible explanation for the greater damping of the large-scale divergence in the DNI schemes could be that the damping characteristics of the scheme used are frequency dependent. Thus, while the high frequency gravity modes are damped greatly, the large-scale low frequency Rossby modes are also damped to some extent. The extent of this undesirable damping of the slow modes varies with the number of forward-backward time integrations used. Sugi[6] depicts very little Rossby mode damping after 100 cycles of the time scheme, but points out that the damping may not be negligible if the time scheme is exercised more than that. In this study, 400 integrations were used, which may explain the more pronounced damping by the DNI scheme in those figures. Sugi suggests that, since the frequency-dependent damping is a direct result of the choice of time integration scheme, it may be possible to design such a scheme with more desirable damping characteristics (more high frequency damping, less low frequency damping). By contrast, the NMI completely damps all modes with periods shorter than 48 hours, while lower frequency (longer period) modes are completely retained. As both the 12- and 15-layer model forecasts progress to 12 and 24 hours, the differences in RMS divergence between the adiabatic and diabatic initialization become less, but the divergence values in the NMI-based forecasts remain greater than those from the DNI-based forecasts.

The purpose of initialization is to eliminate high frequency gravity waves in the forecast that could lead to forecast error, while minimizing the effect on the large-scale motions that would be depicted in the global RMS divergences as shown here. Because the diabatic NMI scheme demonstrates the least amount of large-scale damping, yet results in a forecast just as good as the other schemes, it might be considered the most preferred scheme on the basis of these results. According to this study, and in a globally averaged

sense, the type of initialization (nonlinear normal mode vs dynamic normal mode) appears to have more impact on a model forecast of divergence than the type of physics (adiabatic vs diabatic) used in the initialization. This result is consistent with the conclusions of Errico and Rasch,[15] in which they found a similarly small impact on the forecasts when diabatic effects were included in the initialization. However, the presence of diabatic effects in initialization are likely to become important for tropical regions of the globe, where diabatically driven divergences greatly influence the type of weather there.

Initial time vertical velocities at around 500 mb for the 12Z 17 June 1979 analysis and the initialized states are shown in Figure 17 for the region between 60 degrees north and south in the eastern hemisphere. The large vertical velocity values shown in the analysis are damped significantly by the adiabatic and diabatic NMI and DNI schemes; however, the NMID actually shows an increase in the vertical velocity magnitudes in the tropics near India and the East Indies. This retention of large vertical velocities by NMID in the tropics may be a realistic representation of a strong convective environment. The sophisticated physics in NMID may have helped to strengthen this convection, while the damping characteristics of NMID resulted in less divergence damping (as shown above) and thus yielded greater vertical velocities when compared to the DNI schemes.

Table 3 displays global grid point RMS differences between NMI and DNI forecasts and verification analyses of vertical velocities at around 500 mb for the June case. Differences in magnitude between initialized forecasts and the corresponding analyses are also shown. The decrease in the grid point RMS differences between 0 and 12 hours and the positive magnitude difference (initialized > analysis) reflects the spin-up of vertical velocity in the model after the initial damping of vertical velocity by NMI and DNI. The signifcant increase in the grid point RMS differences beteen 12 and 24 hours is due to random forecast errors, while the magnitude differences become negative (analysis > initialized) as the model spin-up relaxes. This model spin-up helps to relieve the differences that existed between analyzed and initialized vertical velocity at the initial time. However, it is desirable to obtain an initialized state that requires as little spin-up as possible while providing an accurate forecast. Table 3 shows that the AFGL sophisticated physics version of NMI requires the least spin-up, whle the AFGWC physics version of NMI provides the best forecast of vertical velocity in these experiments.

## 4. CONCLUSIONS

The adiabatic and diabatic dynamic normal mode initialized (DNI) forecasts in this study were comparable in accuracy to the adiabatic and diabatic nonlinear normal mode

15. Errico, R.M., and Rasch, P.J. (1988) A comparison of various normal-mode initialization schemes and the inclusion of diabatic processes. *Tellus*, **40A**.

Table 3. Global RMS Differences Between Forecast and Analyzed Vertical Velocity (microbars/sec) for Sigma Level 0.574 (about 500 mb). Differences in magnitude are shown in parentheses

| AFGWC PHYSICS | | | |
|---|---|---|---|
| | HR | ADIABATIC | DIABATIC |
| NMI | 0 | 2.27(-1.42) | 2.61(-1.56) |
| | 12 | 1.53( 0.65) | 1.45( 0.57) |
| | 24 | 2.53(-0.33) | 2.48(-0.40) |
| DNI | 0 | 2.54(-1.56) | 2.36(-1.55) |
| | 12 | 1.39( 0.50) | 1.40( 0.50) |
| | 24 | 2.48(-0.43) | 2.47(-0.43) |
| AFGL PHYSICS | | | |
| | HR | ADIABATIC | DIABATIC |
| NMI | 0 | 2.27(-1.42) | 2.77(-1.35) |
| | 12 | 1.87( 0.87) | 1.90( 0.86) |
| | 24 | 2.87(-0.03) | 3.00(-0.02) |
| DNI | 0 | | 2.52(-1.42) |
| | 12 | 2.54(-1.56) | 1.80( 0.76) |
| | 24 | 1.78( 0.75) | 3.07(-0.05) |
| | | 3.06(-0.07) | |

Figure 17. Initial Time Vertical Velocities ($10^{-3}$ mb s$^{-1}$) at Sigma
Level 0.574 ($\approx$500 mb) for 12Z 17 June 1979 Analysis and
Different Initialization Methods (Positive Values Indicate
Sinking Motion, Negative Values Indicate Rising Motion):
(a) Analysis, (b) NMI
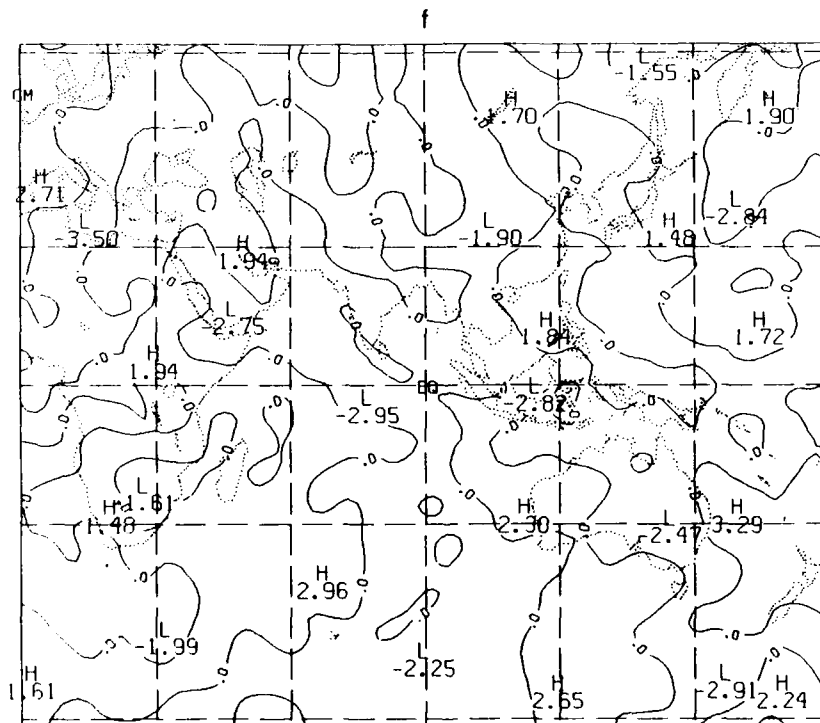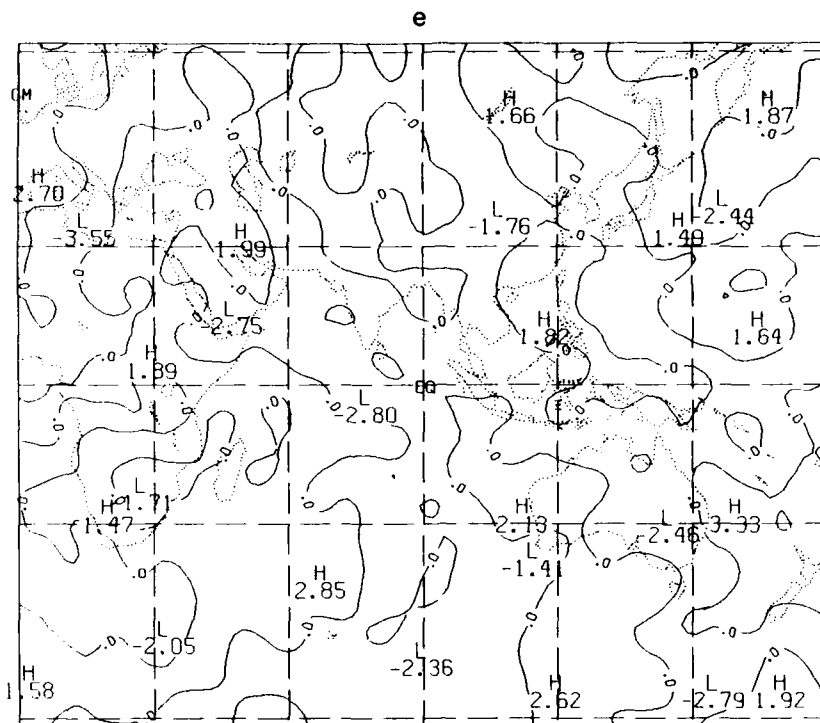
33

Figure 17 (cont). Initial Time Vertical Velocities ($10^{-3}$ mb s$^{-1}$) at Sigma Level 0.574 ($\approx$ 500 mb) for 12Z 17 June 1979 Analysis and Different Initialization Methods (Positive Values Indicate Sinking Motion, Negative Values Indicate Rising Motion): (c) GWC NMID, (d) AFGL (ALL) NMID

34

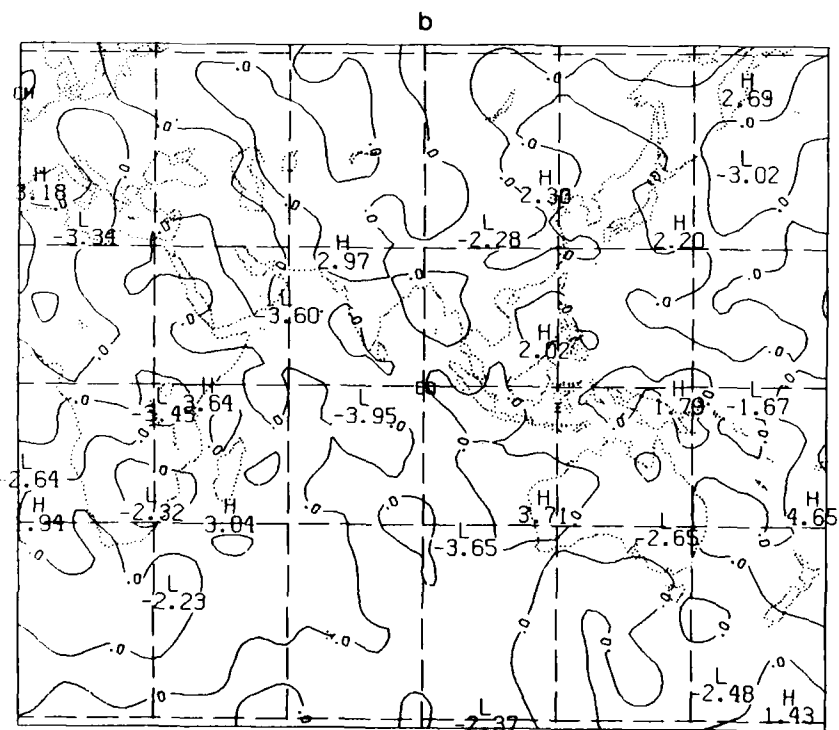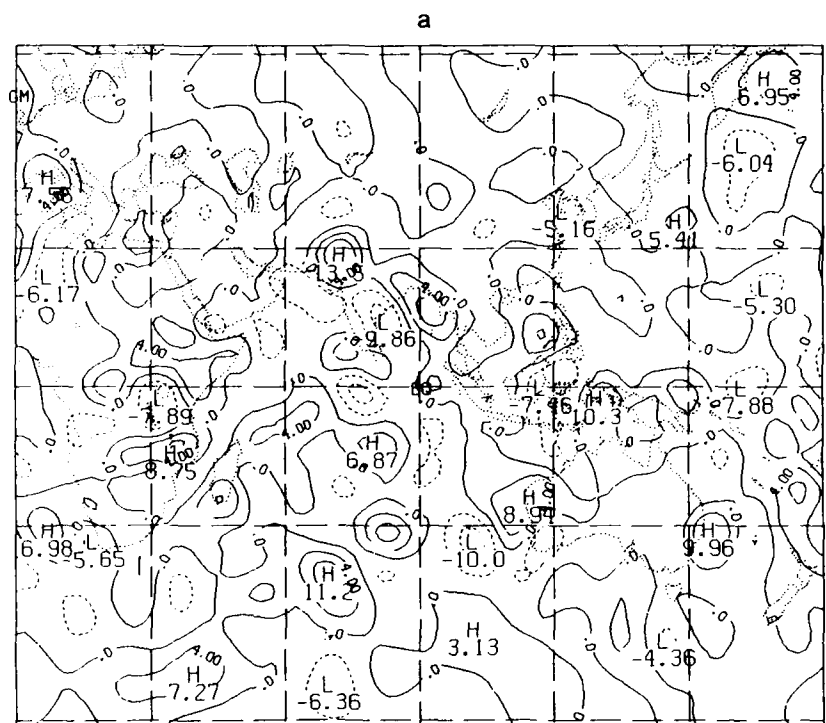Figure 17 (cont). Initial Time Vertical Velocities ($10^{-3}$ mb s$^{-1}$) at Sigma Level 0.574 ($\approx$500 mb) for 12Z 17 June 1979 Analysis and Different Initialization Methods (Positive Values Indicate Sinking Motion, Negative Values Indicate Rising Motion): (e) DNI, (f) GWC DNID

35

g



Figure 17 (cont). Initial Time Vertical Velocities (10$^{-3}$ mb s$^{-1}$) at
Sigma Level 0.574 ($\approx$500 mb) for 12Z 17 June 1979 Analysis
and Different Initialization Methods (Positive Values
Indicate Sinking Motion, Negative Values Indicate Rising
Motion): (g) AFGL (ALL) DNID

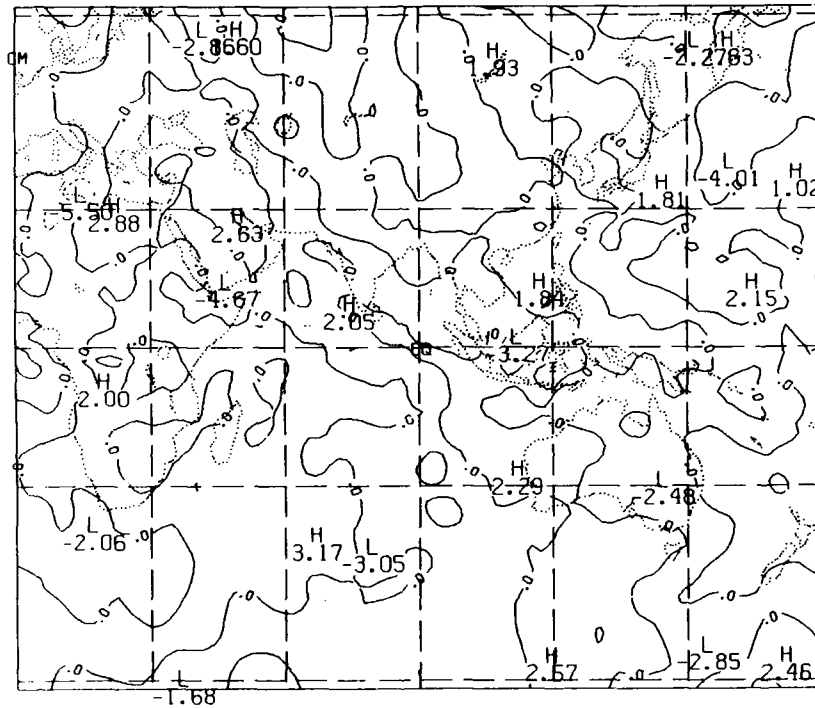36

initialized (NMI) forecasts. Thus, the DNI schemes achieved the goal of initialization in that they provided reasonable forecasts following the elimination of undesirable high frequency gravity waves. Because of the greater likelihood of the DNI process to converge when diabatic effects are included and its more straightforward application to limited area models, the DNI appears to be a satisfactory alternative. However, the time differencing scheme and the number of integrations used in DNI may need to be changed from this study to prevent the damping of resolvable scales of motion that appeared to be evident in this study. Though the differences between adiabatic and diabatic initialization were observed to be small in this study, these differences would grow in time in separate data assimilation procedures; therefore, small differences shown in this study could become significant after repeated applications in a data assimilation sequence. More research with DNI will be required to more completely evaluate its potential effectiveness and utility relative to other initialization schemes.

**References**


1.  Charney, J. (1955) The case of the primitive equations of motion in numerical forecasting. *Tellus*, 7:22-26.


2.  Phillips, N. (1960) On the problem of initial data for the primitive equations. *Tellus*, 12:121-126.


3.  Miyakoda, K., and Moyer, R.W. (1968) A method of initialization for dynamical weather forecasting. *Tellus*, 7:22-26.


4.  Machenhauer, B. (1977) On the dynamics of gravity oscillations in a shallow water model, with application to normal mode initialization. *Beitr. Phys. Atmos.*, 50:253-271.


5.  Daley, R. (1981) Normal mode initialization. *Rev. Geophys. Space Phys.*, 19:450-468.


6.  Sugi, M. (1986) Dynamic normal mode initialization. *J. Meteor. Soc. Japan*, 64:623-626.


7.  Brenner, S., Yang, C.H., and Yee, S.Y.K. (1982) *The AFGL Spectral Model of the Moist Global Atmosphere: Documentation of the Baseline Version.* AFGL-TR-82-0393, Air Force Geophysics Laboratory, Hanscom AFB. [NTIS ADA 129283.]


8.  Ballish, A.B. (1980) *Initialization Theory and Application to the NMC Spectral Model.* Unpublished Ph.D. thesis, Dept. of Meteorology, U. of Maryland.


9.  Sela, J. (1980) Spectral modeling at the National Meteorological Center. *Mon. Wea. Rev.* 108:1279-1292.


10. Sela, J. (1982) *The NMC Spectral Model.* NOAA Technical Report NWS-30.

11. Ou, S.-C., and Liou, K.-N. (1988) *Development of Radiation and Cloud Parameterization Programs for AFGL Global Models.* Final Report, AFGL-TR-87-0246, Air Force Geophysics Laboratory, Hanscom AFB. [NTIS AD A199440].

12. Soong, S.-T., Ogura, Y., and Kau, W.-S. (1985) *A Study of Cumulus Parameterization in a Global Circulation Model.* Final Report, AFGL-TR-85-0160, Air Force Geophysics Laboratory, Hanscom AFB. [NTIS AD A170137].

13. Mahrt, L., Pan, H.-L., Ruscher, P., and Chu, C.-T. (1987) *Boundary Layer Parameterization for a Global Spectral Model.* Final Report, AFGL-TR-87-0246, Air Force Geophysics Laboratory, Hanscom AFB. [NTIS AD A199440].

14. Brenner, S., Yeng, C.H., and Mitchell, K. (1984) *The AFGL Global Spectral Model: Expanded Resolution Baseline Version.* AFGL-TR-84-0308, Air Force Geophysics Laboragory, Hanscom AFG. [NTIS ADA 160370.]

15. Errico, R.M., and Rasch, P.J. (1988) A comparison of various normal-mode initialization schemes and the inclusion of diabatic processes. *Tellus*, **40A**.